IET Communications

Research Article

IET Journals
The Institution of Engineering and Technology

On ASER performance of higher order QAM schemes in two-way multiple-relay networks under imperfect CSI

ISSN 1751-8628
Received on 4th June 2019
Revised 22nd December 2019
Accepted on 29th January 2020
E-First on 29th April 2020
doi: 10.1049/iet-com.2019.0585
www.ietdl.org

Nagendra Kumar[1] ✉, *Praveen Kumar Singya*[2], *Vimal Bhatia*[2]

[1]*Department of Electronics & Communication Engineering, National Institute of Technology Jamshedpur, Adityapur, Jharkhand, Jamshedpur-831014, India*

[2]*Signals and Software Group, Electrical Engineering Department, Indian Institute of Technology Indore, Madhya Pradesh, Indore-453552, India*

✉ *E-mail: kumar.nagendra86@gmail.com*

Abstract: In this study, the authors present an analytical approach to evaluate the performance of a two-way multi-relay system with direct link using a three-phase analogue network coding and opportunistic relay selection scheme. Herein, the imperfect channel state information is considered over independent and non-identically distributed Nakagami-*m* fading channels with integer-valued fading parameter. For analysis, initially, the closed-form expressions of cumulative distribution function and moment generating function (MGF) for the considered system are derived. Further, by using the MGF-based approach, generalised expressions of average symbol error rate (ASER) for higher-order quadrature amplitude modulation (QAM) schemes such as hexagonal QAM, rectangular QAM, and cross QAM are derived. They then analyse the asymptotic behaviour of ASER expression to evaluate the system's diversity order. Furthermore, a comparative analysis of the ASER performance for various QAM constellations is illustrated and impact of the number of relays, fading parameter, relay location, and channel estimation error are highlighted on the system's performance. Finally, all the analytical results are validated through Monte-Carlo simulations.

1 Introduction

Cooperative communication has received significant research interest due to spectrally efficient high data-rate communication with enhanced capacity and coverage for more number of users. In the half-duplex mode of operation, two-way relaying (TWR) is proposed as one of the spectrally efficient schemes [1]. Due to spectral efficiency and low design complexity, analogue network coding (ANC) has tremendously been considered in TWR [2]. With the help of amplify-and-forward (AF) relaying, ANC provides bidirectional communication to both the source terminals with the half-duplex mode of operation. In the literature, many works focus on the two-phase ANC (2P-ANC), where both the source terminals exchange their information in two-time phases. As the direct link between the source terminals is absent in 2P-ANC, diversity performance is poorer than the conventional one-way relaying, despite its spectral efficiency. To improve the performance, a three-phase ANC (3P-ANC) is proposed [3], which exploits the advantage of the direct link between the source terminals. In 3P-ANC, both the source terminals transmit their information in the first and the second time phases, and relay transmits its information in the third time phase. Thus, 3P-ANC improves the system's performance than the 2P-ANC, at the cost of one extra phase.

On the other hand, opportunistic relay selection (ORS) provides full diversity gain with low computational complexity as it selects the best relay link out of the N available relays to improve the system's performance [4]. The literature [5–7] focus on the performance analysis of a TWR network with ORS using 2P-ANC and 3P-ANC, respectively. The analysis considered in [5–7] assume perfect knowledge of the channel state information (CSI) at the nodes. However, in practice, perfect knowledge of the CSI is not available, which results in channel estimation error (CEE), at the receiver. CEE deteriorates system's performance significantly and is required to be addressed for practical system design. Thus, over the years, the impact of CEE on various relay networks is also studied. For 2P-ANC based TWR networks considered in [8, 9], the impact of imperfect CSI is observed on their performances. In [10], for a 2P-ANC based TWR network, diversity-multiplexing trade-off is illustrated in the presence of imperfect CSI. In [11], for a 3P-ANC based two-way multi-relay network over Nakagami-*m* fading links with maximal ratio combining (MRC) receiver, the closed-form expression of outage probability is derived under imperfect CSI. In [12], approximated expressions of outage probability, error probability, and achievable rate are evaluated in a single relay AF-based TWR system considering imperfect CSI. In [13], outage probability, diversity-multiplexing tradeoff, and asymptotic and limiting behaviour of diversity-multiplexing tradeoff are analysed in a TWR system considering 3P-ANC and imperfect CSI. In [14], approximate closed-form expressions of outage probability in AF-based TWR system with residual self-interference are derived when considering both perfect and imperfect CSI. In [15], the outage performance of a full-duplex two-way decode-and-forward (DF) relay network with imperfect CSI is analysed. In [16], the closed-form expressions of outage probability are derived, and the impact of hardware impairments is analysed in AF-based one-way relaying and TWR systems under Rayleigh faded channel when imperfect CSI is considered. In [17], the impact of CEE on the overall outage performance of TWR network with a direct link is analysed for imperfect CSI when ORS is considered. Recently, in [18], the outage probability of AF-based TWR network is derived while multiple co-channel interferences are considered.

Further, data-rate enhancement with optimum power utilisation for a given bandwidth, adaptive modulation plays an important role in wireless communication [19]. Hence, to obtain enhanced data-rate with improved power efficiency, higher-order modulation schemes such as various quadrature amplitude modulation (QAM) schemes (i.e. hexagonal QAM (HQAM), cross QAM (XQAM), and rectangular QAM (RQAM)) have gained tremendous interest in the present and future wireless communication systems. Square QAM (SQAM) is the most commonly used modulation scheme for constellations of even power of 2. For the odd power of 2 constellations, RQAM is commonly preferred due to its generalised nature as various modulation schemes are its special cases [20]. However, RQAM is not a good choice due to its high peak and average energies, and instead, a modified structure termed as XQAM is preferred due to its lower peak and average energies than

RQAM. Outer corner points of RQAM constellations are moved to a new position to obtain XQAM structure such that average energy of the constellation is minimised and thus, XQAM provides significant signal-to-noise ratio (SNR) gain over the RQAM scheme [21]. On the other hand, because of the densest 2D packing and optimum Euclidean distance in a hexagonal lattice, HQAM has a comparatively lower peak and average energies, and thus, is more energy-efficient than SQAM, RQAM, and XQAM schemes.

Recently, considerable work on the performance analysis of higher-order modulation schemes in various communication systems has been reported in the literature. For regular, optimum, and sub-optimum triangular QAM (TQAM) schemes, generalised bit error rate expression is derived in [19], and a comparative analysis of detection complexity between them is presented. In [20], a non-relay multi-branch system over independent but not necessarily identically distributed (i.n.i.d.) Nakagami-*m* fading channels is considered, and exact average symbol error rate (ASER) expressions of RQAM, differentially encoded quadrature phase-shift keying (De-QPSK) and $\pi/4$-QPSK are derived. For a multi-relay system, the closed-form ASER expressions of RQAM, XQAM, HQAM, De-QPSK, and $\pi/4$-QPSK schemes over i.n.i.d. Nakagami-*m* fading links are derived in [21]. In [22], a single relay AF network over i.n.i.d. Nakagami-*m* fading links with imperfect CSI is considered and the closed-form expressions of outage probability, asymptotic outage probability, and ASER of both HQAM and RQAM schemes are derived. In [23], for a non-relay system, generalised symbol error probability expression for HQAM scheme over Rayleigh fading link is derived. Further, in [24–26], for non-relay systems over additive white Gaussian noise (AWGN) channel, ASER performance of various TQAM (or HQAM) constellations are analysed.

To the best of authors' knowledge, no work in the literature focuses on the ASER performance of the higher-order QAM schemes, especially in TWR networks. Therefore, for the first time in the literature, novel closed-form expressions of ASER for *M*-ary HQAM, *M*-ary RQAM, and *M*-ary XQAM schemes are derived in TWR network considering 3P-ANC with imperfect CSI under versatile i.n.i.d. Nakagami-*m* faded environment using moment generating function (MGF) based approach. Further, asymptotic ASER expression is derived to investigate the diversity order of the considered system. Furthermore, the impact of fading parameter, number of relays, CEE and relay location on ASER performance are highlighted. Therefore, because of considering a more reliable spectrally efficient two-way multi-relay network, more bandwidth, and energy-efficient higher-order QAM schemes, more realistic system (imperfect CSI), and versatile channel environment, the covered work in this manuscript will be of keen interest for the fifth-generation (5G) and beyond communications to provide high reliability, large coverage and high throughput.

2 System and channel model

In this work, we consider a two-way multi-relay system with direct link using 3P-ANC and ORS scheme. For the considered system, two sources S_1 and S_2 exchange their informations via direct link, and also with the aid of N relay nodes R_n, $n = 1, 2, \ldots, N$, as shown in Fig. 1. Single antenna and half-duplex deployments are considered at all the communication nodes. Further, quasi-static and reciprocal channels are considered over i.n.i.d. Nakagami-*m* faded channels with integer valued fading parameter for all the links. Channel coefficient of direct link is denoted by H_0 and is modelled as $\text{Nak}(m_0, \sigma_0^2)$. Further, the channel coefficients of the links between ith source and nth relay, and jth source and nth relay are denoted by H_{in} and H_{jn}, respectively, where $i, j \in \{1, 2\}$ with $i \neq j$. Furthermore, channel coefficients of the corresponding links are modelled as $\text{Nak}(m_{in}, \sigma_{in}^2)$ and $\text{Nak}(m_{jn}, \sigma_{jn}^2)$, respectively. Here, $\text{Nak}(m_l, \sigma_l^2)$ represents the Nakagami-*m* distribution with m_l fading severity and σ_l^2 variance where $l \in \{in, jn, 0\}$. P_s and P_r represent transmit power at both the sources and all the relays, respectively. It is assumed that the CSI is unknown to the source and relay nodes, thus, minimum mean squared error (MMSE) estimation is used at the receiving nodes. Here, H_l and $\hat{H}_l$ represent channel

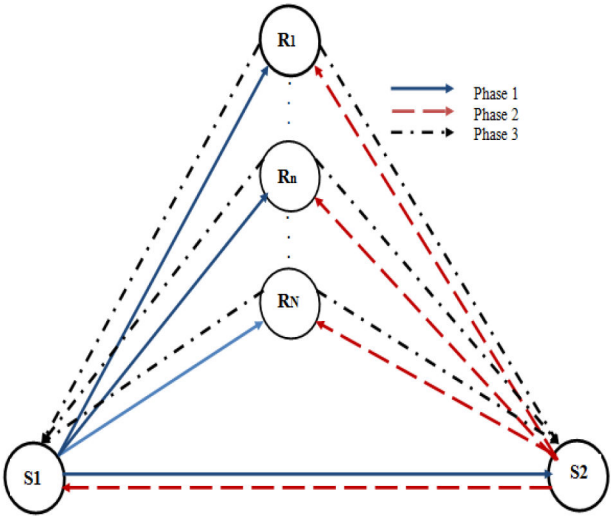

Fig. 1 *System model*

coefficient and estimated value of channel coefficient, respectively. As MMSE estimation is preferred, the channel coefficient and its estimated value are related as $H_l = \hat{H}_l + E_l$. Thus, variances of actual channel and its estimated version are related as $\sigma_{H_l}^2 = \sigma_{\hat{H}_l}^2 + \sigma_{E_l}^2$, where E_l is the complex Gaussian CEE with zero mean and variance $\sigma_{E_l}^2 = (\sigma_{H_l}^2/(1 + \rho\bar{\lambda}_\text{a}\sigma_{H_l}^2))$ wherein $\rho > 0$ is the quality of channel estimation [10, 11]. Further, $\bar{\lambda}_\text{a} = P_\text{s}/\sigma^2$ is the average transmit SNR.

In the considered system, communication between all nodes is completed in three time phases. In the first time phase, S_1 transmits the signal X_1 with transmitted power P_s, and hence, we can express the received signal at S_2 and R_n as

$$Y_{S_2}^{(\text{I})} = \sqrt{P_\text{s}}(\hat{H}_0 + E_0)X_1 + \eta_{S_2}^{(\text{I})}, \tag{1}$$

$$Y_{R_n}^{(\text{I})} = \sqrt{P_\text{s}}(\hat{H}_{1n} + E_{1n})X_1 + \eta_{R_n}^{(\text{I})}, \tag{2}$$

respectively, where $\eta_{S_2}^{(\text{I})}$ and $\eta_{R_n}^{(\text{I})}$ represent complex AWGNs with zero mean and variance σ^2 at S_2 and R_n nodes, respectively. In the second time phase, S_2 transmits the signal X_2 with power P_s, and hence the received signals at S_1 and R_n can be represented as

$$Y_{S_1}^{(\text{II})} = \sqrt{P_\text{s}}(\hat{H}_0 + E_0)X_2 + \eta_{S_1}^{(\text{II})}, \tag{3}$$

$$Y_{R_n}^{(\text{II})} = \sqrt{P_\text{s}}(\hat{H}_{2n} + E_{2n})X_2 + \eta_{R_n}^{(\text{II})}, \tag{4}$$

respectively, where $\eta_{S_1}^{(\text{II})}$ and $\eta_{R_n}^{(\text{II})}$ are complex AWGNs with zero mean and variance σ^2 at respective nodes. During the third time phase, relay node R_n combines the received signal $Y_{R_n}^{(\text{I})}$ and $Y_{R_n}^{(\text{II})}$ by employing TWR ANC as $X_{R_n} = \mathcal{G}_n[\sqrt{\mathcal{B}_{1n}}Y_{R_n}^{(\text{I})} + \sqrt{\mathcal{B}_{2n}}Y_{R_n}^{(\text{II})}]$, and then broadcasts the combined signal with power P_r. Thus, the received signal at ith source is represented as

$$\begin{aligned} Y_{S_{in}}^{\text{III}} = {} & \mathcal{G}_n(\hat{H}_{in} + E_{in})[\sqrt{\mathcal{B}_{in}P_\text{s}}(\hat{H}_{in} + E_{in})X_i \\ & + \sqrt{\mathcal{B}_{jn}P_\text{s}}(\hat{H}_{jn} + E_{jn})X_j + \sqrt{\mathcal{B}_{in}}\eta_{R_n}^{(\text{I})} \\ & + \sqrt{\mathcal{B}_{jn}}\eta_{R_n}^{(\text{II})}] + \eta_{S_i}^{(\text{III})}, \end{aligned} \tag{5}$$

where $\sqrt{\mathcal{B}_{1n}}$ and $\sqrt{\mathcal{B}_{2n}}$ are non-negative power allocation factors with $\mathcal{B}_{1n} + \mathcal{B}_{2n} = 1$. Amplification factor at R_n is

$$\mathcal{G}_n = \sqrt{\frac{P_\text{r}}{\mathcal{B}_{1n}P_\text{s}(\left|\hat{H}_{1n}\right|^2 + \sigma_{E_{1n}}^2) + \mathcal{B}_{2n}P_\text{s}(\left|\hat{H}_{2n}\right|^2 + \sigma_{E_{2n}}^2}}$$

and $\eta_{S_i}^{(\mathrm{III})}$ is the complex AWGN with zero mean and variance σ^2 at S_i. As S_i knows its own transmitted signal X_i and estimate of channel coefficients, self-interference terms can be neglected [17]. Thus, we can express the resulting signal at S_i as

$$\begin{aligned}\tilde{Y}_{S_{in}}^{\mathrm{III}} = {} & \mathcal{G}_n\sqrt{\mathcal{B}_{jn}P_{\mathrm{s}}}\hat{H}_{in}\hat{H}_{jn}X_j + \mathcal{G}_n\sqrt{\mathcal{B}_{in}P_{\mathrm{s}}}(2\hat{H}_{in}E_{in} \\ & + E_{in}^2)X_i + \mathcal{G}_n\sqrt{\mathcal{B}_{jn}P_{\mathrm{s}}}(\hat{H}_{in}E_{jn} + \hat{H}_{jn}E_{in} \\ & + E_{in}E_{jn})X_j + \mathcal{G}_n(\hat{H}_{in} + E_{in})(\sqrt{\mathcal{B}_{in}}\eta_{R_n}^{(\mathrm{I})} \\ & + \sqrt{\mathcal{B}_{jn}}\eta_{R_n}^{(\mathrm{II})}) + \eta_{S_i}^{(\mathrm{III})}\end{aligned} \tag{6}$$

From (6), we can express the instantaneous SNR at S_i through nth relay link as

$$\lambda_{S_{in}} = \frac{\hat{\lambda}_{in}\hat{\lambda}_{jn}}{\tau_1\hat{\lambda}_{in} + \tau_2\hat{\lambda}_{jn} + \tau_3} \tag{7}$$

where $\tau_1 = (1/\mathcal{B}_{jn})\{4\mathcal{B}_{in}\epsilon_{in} + \mathcal{B}_{jn}\epsilon_{jn} + 2\mathcal{B}_{in} + \mathcal{B}_{jn}\}$, $\tau_2 = (1/\mathcal{B}_{jn})\{\mathcal{B}_{jn}\epsilon_{in} + \mathcal{B}_{jn}\}$, $\tau_3 = (1/\mathcal{B}_{jn})\{\mathcal{B}_{in}\epsilon_{in}^2 + \mathcal{B}_{jn}\epsilon_{in}\epsilon_{jn} + 2\mathcal{B}_{in}\epsilon_{in} + \mathcal{B}_{jn}\epsilon_{in} + \mathcal{B}_{jn}\epsilon_{jn} + 1\}$, $\hat{\lambda}_{in} = P_{\mathrm{s}}\left|\hat{H}_{in}\right|^2/\sigma^2$, $\hat{\lambda}_{jn} = P_{\mathrm{r}}\left|\hat{H}_{jn}\right|^2/\sigma^2$, $\epsilon_{in} = P_{\mathrm{s}}\sigma_{E_{in}}^2/\sigma^2$, $\epsilon_{jn} = P_{\mathrm{r}}\sigma_{E_{jn}}^2/\sigma^2$. As it is assumed that the estimation error and noise variances are small in practice, τ_3 can be removed from (7) for analytical simplicity. Further, ORS algorithm is adopted at S_i hence, a relay with highest SNR (n^*) is selected as $\lambda_{n^*} = \mathrm{argmax}_{n\in\{1,\ldots,N\}}\{\lambda_n\}$ [27, 28], where

$$\lambda_n = \min\left(\frac{\hat{\lambda}_{in}}{\tau_2}, \frac{\hat{\lambda}_{jn}}{\tau_1}\right)$$

is the upper-bound of $\lambda_{S_{in}}$. Furthermore, MRC scheme is considered for best relay link and direct link at S_i. Thus, upper-bound of the end-to-end SNR, λ_{S_i} can be expressed as

$$\lambda_{S_i} \le \lambda_0 + \lambda_{n^*}, \tag{8}$$

where $\lambda_0 = \hat{\lambda}_0/((1+\epsilon_0))$ is the instantaneous SNR of the direct link, $\hat{\lambda}_0 = P_{\mathrm{s}}\left|\hat{h}_0\right|^2/\sigma^2$, and $\epsilon_0 = P_{\mathrm{s}}\sigma_{E_0}^2/\sigma^2$. As we consider Nakagami-m fading for all the wireless links, the probability density function (PDF) and the cumulative distribution function (CDF) expressions for Nakagami-m distributed lth link can be represented as

$$f_{\lambda_l}(\lambda) = \left(\frac{m_l}{\bar{\lambda}_l}\right)^{m_l}\frac{\lambda^{m_l-1}}{\Gamma[m_l]}\mathrm{e}^{-\frac{m_l}{\bar{\lambda}_l}\lambda} \text{ and}$$

$$F_{\lambda_l}(\lambda) = 1 - \frac{1}{\Gamma[m_l]}\Gamma\left(m_l, \frac{m_l}{\bar{\lambda}_l}\lambda\right),$$

respectively, where $\bar{\lambda}_l$, $\Gamma[\cdot]$ and $\Gamma(\cdot,\cdot)$ represent average SNR of lth link, Gamma, and upper incomplete Gamma functions, respectively. Further, we can formulate the lower-bound expression of CDF for λ_{S_i} as [29, eq. (25)]

$$F_{\lambda_{S_i}}(\lambda) = \int_0^\infty f_{\lambda_0}(\phi)F_{\lambda_{n^*}}(\lambda-\phi)\,\mathrm{d}\phi, \tag{9}$$

where $F_{\lambda_{n^*}}(\lambda)$ can be given as

$$F_{\lambda_{n^*}}(\lambda) = \prod_{n=1}^{N}\left(1 - [1 - F_{\hat{\lambda}_{in}}(\tau_2\lambda)][1 - F_{\hat{\lambda}_{jn}}(\tau_1\lambda)]\right). \tag{10}$$

Substituting the CDF of corresponding links into (10) and after some mathematical calculations, we get

$$\begin{aligned}F_{\lambda_{n^*}}(\lambda) = {} & 1 + \sum_{n=1}^{N}\binom{N}{n}(-1)^n\left(\frac{\Gamma(m_{in}, \frac{m_{in}}{\hat{\lambda}_{in}}\tau_2\lambda)}{\Gamma(m_{in})}\right)^n \\ & \times\left(\frac{\Gamma(m_{jn}, \frac{m_{jn}}{\hat{\lambda}_{jn}}\tau_1\lambda)}{\Gamma(m_{jn})}\right)^n.\end{aligned} \tag{11}$$

Further, alternate form of upper incomplete gamma function

$$\left[\frac{\Gamma(m_l, \tau\lambda)}{\Gamma(m_l)}\right]^n = \mathrm{e}^{-n\tau\lambda}\left[\sum_{\iota=0}^{m_l-1}\frac{(\tau\lambda)^\iota}{\iota!}\right]^n$$

is used and then the multinomial is expanded as $[\sum_{\iota=0}^{m_l-1}(w_\iota\lambda^\iota)]^n = \sum_{\iota=0}^{n(m_l-1)}w_\iota^n\lambda^\iota$, where the coefficient w_ι^n can be recursively calculated using [30, eq. (0.314)]. By substituting multinomial expansion in (11), the simplified form of $F_{\lambda_{n^*}}(\lambda)$ can be expressed as

$$\begin{aligned}F_{\lambda_{n^*}}(\lambda) = {} & 1 + \sum_{n=1}^{N}\binom{N}{n}(-1)^n\sum_{k_1=0}^{n(m_{in}-1)}\sum_{k_2=0}^{n(m_{jn}-1)}w_{k_1}^n \\ & \times w_{k_2}^n\left(\frac{m_{in}\tau_2}{\hat{\lambda}_{in}}\right)^{k_1}\left(\frac{m_{jn}\tau_1}{\hat{\lambda}_{jn}}\right)^{k_2}\lambda^{k_1+k_2} \\ & \times\mathrm{e}^{-n\left(\frac{m_{in}\tau_2}{\hat{\lambda}_{in}} + \frac{m_{jn}\tau_1}{\hat{\lambda}_{jn}}\right)\lambda},\end{aligned} \tag{12}$$

where coefficient w_k^n is calculated as $w_0^n = (z_0)^n$, $w_1^n = n(z_1)$ and $w_{n(m-1)}^n = (z_{m-1})^n$ for $0 \le k \le n(m-1)$, $w_k^n = (1/kz_0)\sum_{q=1}^{k}[qn-k+q]z_q w_{k-q}^n$ for $2 \le k \le m-1$, and $w_k^n = (1/kz_0)\sum_{q=1}^{m-1}[qn-k+q]z_q w_{k-q}^n$ for $m \le k \le n(m-1)$ with $z_k = 1/k!$. Substituting the PDF expression of direct link $f_{\lambda_0}(\phi)$, and the CDF expression $F_{\lambda_{n^*}}(\lambda-\phi)$ into (9), then using binomial expansion and [30, eq. (3.351)], and further solving, we get

$$\begin{aligned}F_{\lambda_{S_i}}(\lambda) = {} & \left[1 - \frac{\Gamma(m_0, \mu_1\lambda)}{\Gamma(m_0)}\right] + \Xi_1\lambda^{k_1+k_2-l_1}\mathrm{e}^{-n\mu_2\lambda} \\ & -\Xi_2\lambda^{k_1+k_2-l_1+l_2}\mathrm{e}^{-\mu_1\lambda},\end{aligned} \tag{13}$$

where $\Xi_1 = \sum_{n=1}^{N}\binom{N}{n}(-1)^n\sum_{k_1=0}^{n(m_{in}-1)}\sum_{k_2=0}^{n(m_{jn}-1)}w_{k_1}^n w_{k_2}^n(m_{in}\tau_2/\hat{\lambda}_{in})^{k_1}$, $(m_{jn}\tau_1/\hat{\lambda}_{jn})^{k_2}\sum_{l_1=0}^{k_1+k_2}\binom{k_1+k_2}{l_1}(-1)^{l_1}(\mu_1-n\mu_2)^{-(m_0+l_1)}\Gamma(m_0+l_1)$
$\Xi_2 = \Xi_1\sum_{l_2=0}^{m_0+l_1-1}\frac{1}{l_2!}(\mu_1-n\mu_2)^{l_2}$,

$$\mu_1 = \frac{m_0(1+\epsilon_0)}{\hat{\lambda}_0} \quad \text{and} \quad \mu_2 = n\left(\frac{m_{in}\tau_2}{\hat{\lambda}_{in}} + \frac{m_{jn}\tau_1}{\hat{\lambda}_{jn}}\right).$$

Further, to evaluate the MGF expression for received SNR λ_{S_i}, we can use CDF-based approach as [31, eq. (18)]

$$\mathcal{M}_{\lambda_{S_i}}(s) = \mathbb{E}[\mathrm{e}^{-s\lambda_{S_i}}] = \int_0^\infty s\,\mathrm{e}^{-s\lambda}F_{\lambda_{S_i}}(\lambda)\,\mathrm{d}\lambda, \tag{14}$$

where $\mathbb{E}[\cdot]$ represents the expectation operator. By substituting $F_{\lambda_{S_i}}(\lambda)$ from (13) into (14), and then solving the integral with the aid of [30, eq. (3.351), eq. (6.451)], we get

$$\begin{aligned}\mathcal{M}_{\lambda_{S_i}}(s) = {} & \underbrace{\left[1 + \frac{s}{\mu_1}\right]^{-m_0}}_{\mathcal{M}_{\lambda_1}} + \Xi_1\Phi_1\underbrace{s\left[1 + \frac{s}{n\mu_2}\right]^{-(k_1+k_2-l_1+1)}}_{\mathcal{M}_{\lambda_2}} \\ & -\Xi_2\Phi_2\underbrace{s\left[1 + \frac{s}{\mu_1}\right]^{-(k_1+k_2-l_1+l_2+1)}}_{\mathcal{M}_{\lambda_3}}\end{aligned} \tag{15}$$

where $\Phi_1 = \frac{\Gamma(k_1+k_2-l_1+1)}{(n\mu_1)^{k_1+k_2-l_1+1}}$ and $\Phi_2 = \frac{\Gamma(k_1+k_2-l_1+l_2+1)}{(n\mu_2)^{k_1+k_2-l_1+l_2+1}}$.

3 ASER performance

ASER expression of the considered system for various modulation schemes can be formulated as

$$\mathscr{P}_s(e) = \int_0^\infty \mathscr{P}_s(e\,|\,\lambda) f_{\lambda_{S_i}}(\lambda)\,\mathrm{d}\lambda, \tag{16}$$

where $\mathscr{P}_s(e\,|\,\lambda)$ and $f_{\lambda_{S_i}}(\lambda)$ are the conditional symbol error rate (SER) for AWGN channels, and the PDF of the received SNR, respectively.

3.1 M-ary hexagonal QAM scheme

The conditional SER expression for general order HQAM scheme under AWGN channels is given as [23, eq. (6)]

$$\begin{aligned}\mathscr{P}_s^{\mathrm{HQAM}}(e\,|\,\lambda) = {} & \mathscr{K}\mathscr{Q}(\sqrt{\alpha\lambda}) + \frac{2}{3}\mathscr{K}_c\mathscr{Q}^2\left(\sqrt{\frac{2\alpha\lambda}{3}}\right) \\ & -2\mathscr{K}_c\mathscr{Q}\left(\sqrt{\alpha\lambda}\right)\mathscr{Q}\left(\sqrt{\frac{\alpha\lambda}{3}}\right),\end{aligned} \tag{17}$$

where the numerical values of the parameters $\mathscr{K}$, $\mathscr{K}_c$, and α for different constellations are given in [23] and $\mathscr{Q}(\cdot)$ is the Gaussian $\mathscr{Q}$-function expressed as $\mathscr{Q}(x) = (1/\sqrt{2\pi})\int_x^\infty \mathrm{e}^{-t^2/2}\,\mathrm{d}t$. For the ease of analysis, we can use the alternate form of 1D and 2D Gaussian $\mathscr{Q}$-function as

$$\mathscr{Q}_z(x,\phi) = \frac{1}{\pi}\int_0^\phi \exp\Big(-\frac{x^2}{2\sin^2\theta}\Big)\,\mathrm{d}\theta, \quad x>0. \tag{18}$$

By using (18), we can express $\mathscr{Q}(x) = \mathscr{Q}_z(x,\frac{\pi}{2})$ [30, eq. (4.2)], and $\mathscr{Q}(x)\mathscr{Q}(y) = \frac{1}{2}[\mathscr{Q}_z(x,\frac{\pi}{2}-\arctan(\frac{y}{x})) + \mathscr{Q}_z(y,\arctan(\frac{y}{x}))]$ [32, eq. (4.8)] for $x>0$, $y>0$. Further, with the aid of (18), we can re-express (17) as

$$\begin{aligned}\mathscr{P}_s^{\mathrm{HQAM}}(e\,|\,\lambda) = {} & \mathscr{K}\mathscr{Q}_z(\sqrt{\alpha\lambda},\frac{\pi}{2}) + \frac{2}{3}\mathscr{K}_c\mathscr{Q}_z(\sqrt{\frac{2\alpha\lambda}{3}},\frac{\pi}{4}) \\ & -\mathscr{K}_c[\mathscr{Q}_z(\sqrt{\alpha\lambda},\frac{\pi}{2}-\arctan(\frac{1}{\sqrt{3}})) \\ & +\mathscr{Q}_z(\sqrt{\frac{\alpha\lambda}{3}},\arctan(\frac{1}{\sqrt{3}}))]\,.\end{aligned} \tag{19}$$

Substituting (19) into (16) and by mathematical manipulations, we can formulate the ASER expression for HQAM scheme as

$$\begin{aligned}\mathscr{P}_s^{\mathrm{HQAM}}(e) = {} & \mathscr{K}\mathscr{I}\left(\sqrt{\alpha},\frac{\pi}{2}\right) + \frac{2}{3}\mathscr{K}_c\mathscr{I}\left(\sqrt{\frac{2\alpha}{3}},\frac{\pi}{4}\right) \\ & -\mathscr{K}_c\Big[\mathscr{I}\left(\sqrt{\alpha},\frac{\pi}{2}-\arctan\left(\frac{1}{\sqrt{3}}\right)\right) \\ & +\mathscr{I}\left(\sqrt{\frac{\alpha}{3}},\arctan\left(\frac{1}{\sqrt{3}}\right)\right)\Big],\end{aligned} \tag{20}$$

where the function $\mathscr{I}(\cdot,\cdot)$ is defined in terms of MGF as

$$\begin{aligned}\mathscr{I}(\mathscr{C},\phi) &= \int_0^\infty \mathscr{Q}_z(\mathscr{C}\sqrt{\lambda},\phi) f_{\lambda_{S_i}}(\lambda)\,\mathrm{d}\lambda \\ &= \frac{1}{\pi}\int_0^\phi\int_0^\infty \exp\Big(-\frac{\mathscr{C}^2\lambda}{2\sin^2\theta}\Big) f_{\lambda_{S_i}}(\lambda)\,\mathrm{d}\lambda\,\mathrm{d}\theta \\ &= \frac{1}{\pi}\int_0^\phi \mathscr{M}_{\lambda_{S_i}}\left(\frac{\mathscr{C}^2}{2\sin^2\theta}\right)\mathrm{d}\theta\,.\end{aligned} \tag{21}$$

By substituting (15) into (21), we derive the closed-form expressions for $\mathscr{I}(\sqrt{\alpha},\frac{\pi}{2})$, $\mathscr{I}(\sqrt{\frac{2\alpha}{3}},\frac{\pi}{4})$, $\mathscr{I}(\sqrt{\alpha},\frac{\pi}{2}-\arctan(\frac{1}{\sqrt{3}}))$, and $\mathscr{I}(\sqrt{\frac{\alpha}{3}},\arctan(\frac{1}{\sqrt{3}}))$ by using (30)–(33) respectively, given in Appendix 1. Further, substituting these expressions in (20) and simplifying the resulting expression, we can derive the closed-form expression of ASER for HQAM scheme in Appendix 2 as shown in (37), where ${}_2F_1(\cdot,\cdot,\cdot;\cdot)$ and $F_1(\cdot,\cdot,\cdot;\cdot;\cdot;\cdot)$ represent Gauss hypergeometric function and Appell's double hypergeometric function, respectively.

3.2 M-ary rectangular QAM scheme

The conditional SER expression of M-ary RQAM scheme under AWGN channels is represented as [20, eq. (6)]

$$\begin{aligned}\mathscr{P}_s^{\mathrm{RQAM}}(e\,|\,\lambda) = {} & 2\,p\,\mathscr{Q}(a\sqrt{\lambda}) + 2\,q\,\mathscr{Q}(b\sqrt{\lambda}) \\ & -4\,p\,q\,\mathscr{Q}(a\sqrt{\lambda})\,\mathscr{Q}(b\sqrt{\lambda}),\end{aligned} \tag{22}$$

where $M = M_I \times M_Q$, M_I and M_Q represent the number of in-phase and quadrature-phase constellation points, respectively, $p = 1-(1/M_I)$, $q = 1-(1/M_Q)$,

$$a = \sqrt{\frac{6}{(M_I^2-1)+(M_Q^2-1)\beta^2}},$$

$b = \beta a$ and $\beta = d_Q/d_I$, wherein d_I and d_Q are in-phase and quadrature phase decision distance, respectively. Further, by using (18), we can re-express (22) as

$$\begin{aligned}\mathscr{P}_s^{\mathrm{RQAM}}(e\,|\,\lambda) = {} & 2\,p\,\mathscr{Q}_z\left(a\sqrt{\lambda},\frac{\pi}{2}\right) + 2\,q\,\mathscr{Q}_z\left(b\sqrt{\lambda},\frac{\pi}{2}\right) \\ & -2\,p\,q\left[\mathscr{Q}_z\left(a\sqrt{\lambda},\frac{\pi}{2}-\arctan\left(\frac{b}{a}\right)\right)\right. \\ & \left.+\mathscr{Q}_z\left(b\sqrt{\lambda},\arctan\left(\frac{b}{a}\right)\right)\right].\end{aligned} \tag{23}$$

By substituting (23) into (16) and using some algebraic simplifications, we can formulate ASER expression for the general order RQAM scheme as

$$\begin{aligned}\mathscr{P}_s^{\mathrm{RQAM}}(e) = {} & 2\,p\,\mathscr{I}\left(a,\frac{\pi}{2}\right) + 2\,q\,\mathscr{I}\left(b,\frac{\pi}{2}\right) - 2\,p\,q\Big[\mathscr{I}\Big(a,\frac{\pi}{2} \\ & -\arctan\left(\frac{b}{a}\right)\Big) + \mathscr{I}\left(b,\arctan\left(\frac{b}{a}\right)\right)\Big].\end{aligned} \tag{24}$$

With the help of (30), (32), and (33) given in Appendix 1, we can derive the expressions for $\mathscr{I}(a,\frac{\pi}{2})$, $\mathscr{I}(b,\frac{\pi}{2})$, $\mathscr{I}(a,\frac{\pi}{2}-\arctan(\frac{b}{a}))$, and $\mathscr{I}(b,\arctan(\frac{b}{a}))$. Further, substituting these expressions in (24), the ASER expression for general order RQAM scheme can be obtained in Appendix 2 as shown in (38). By using (38), we can obtain ASER expression for SQAM as a special case by substituting $M_I = M_Q = \sqrt{M}$ and $\beta = 1$. The ASER expression for BPSK can also be obtained from (38) by substituting $M_I = 2$, $M_Q = 1$, $p = 0.5$, $q = 0$, $a = \sqrt{2}$ and $\beta = 0$.

3.3 M-ary cross QAM scheme

The conditional SER for general order XQAM scheme under AWGN channel can be expressed as [33, eq. (15)]

$$\begin{aligned}\mathscr{P}_s^{\mathrm{XQAM}}(e\,|\,\lambda) = {} & \mathscr{U}\,\mathscr{Q}_z\left(\mathscr{A}_0\sqrt{\lambda},\frac{\pi}{2}\right) + \frac{4}{M}\,\mathscr{Q}_z\left(\mathscr{A}_1\sqrt{\lambda},\frac{\pi}{2}\right) \\ & -\mathscr{V}\,\mathscr{Q}_z\left(\mathscr{A}_0\sqrt{\lambda},\frac{\pi}{4}\right) - \frac{8}{M}\sum_{t=1}^{\nu-1}\mathscr{Q}_z(\mathscr{A}_0\sqrt{\lambda},\kappa_t) \\ & -\frac{4}{M}\sum_{t=1}^{\nu-1}\mathscr{Q}_z(\mathscr{A}_t\sqrt{\lambda},\omega_t^+) + \frac{4}{M}\sum_{t=2}^{\nu}\mathscr{Q}_z(\mathscr{A}_t\sqrt{\lambda},\omega_t^-),\end{aligned} \tag{25}$$

where $M = 2^5, 2^7, \ldots,$ $\mathscr{U} = 4 - (6/\sqrt{2M})$, $\mathscr{V} = 4 - (12/\sqrt{2M}) + (12/M)$, $\nu = \frac{2M}{8}$, $\mathscr{A}_0 = \sqrt{96/(31M - 32)}$, $\mathscr{A}_t = \sqrt{2t}\mathscr{A}_0$ for $t = 1, 2, \ldots, \nu$, $\kappa_t = \arctan(1/(2t+1))$ for $t = 1, 2, \ldots, \nu - 1$, $\omega_t^- = \arctan(t/(t-1))$ for $t = 2, 3, \ldots, \nu$ and $\omega_t^+ = \arctan(t/(t+1))$ for $t = 1, 2, \ldots, \nu - 1$. Substituting (25) into (16) and by using some algebraic manipulations, we can express ASER expression for general order XQAM scheme as

$$\begin{aligned}\mathscr{P}_s^{\mathrm{XQAM}}(e) = \mathscr{U}\,\mathscr{I}\Big(\mathscr{A}_0, \frac{\pi}{2}\Big) + \frac{4}{M}\,\mathscr{I}\Big(\mathscr{A}_1, \frac{\pi}{2}\Big) \\ -\mathscr{V}\,\mathscr{I}\Big(\mathscr{A}_0, \frac{\pi}{4}\Big) - \frac{8}{M}\sum_{t=1}^{\nu-1}\mathscr{I}(\mathscr{A}_0, \kappa_t) \\ -\frac{4}{M}\sum_{t=1}^{\nu-1}\mathscr{I}(\mathscr{A}_t, \omega_t^+) + \frac{4}{M}\sum_{t=2}^{\nu}\mathscr{I}(\mathscr{A}_t, \omega_t^-)\,.\end{aligned} \tag{26}$$

To obtain the closed-form expression of (26), we need the values of $\mathscr{I}(\mathscr{A}_0, \frac{\pi}{2})$, $\mathscr{I}(\mathscr{A}_1, \frac{\pi}{2})$, $\mathscr{I}(\mathscr{A}_0, \frac{\pi}{4})$, $\mathscr{I}(\mathscr{A}_0, \kappa_t)$, $\mathscr{I}(\mathscr{A}_t, \omega_t^+)$, and $\mathscr{I}(\mathscr{A}_t, \omega_t^-)$ which can be derived by using (30), (31), (34)–(36) as given in Appendix 1. Further, substituting these expressions into (26), we derive the ASER expression for general order XQAM scheme as shown in (39) in Appendix 2.

3.4 Asymptotic ASER (diversity order)

To examine diversity order of the considered two-way 3P-ANC multi-relay system, we obtain ASER expression for HQAM in the high SNR regime ($\bar{\lambda}_a \to \infty$). Firstly, substituting approximated CDF of corresponding link into (10) by making use of the approximation

$$\frac{\Gamma(\nu, z)}{\Gamma(\nu)} \underset{z \to 0}{\simeq} 1 - \frac{z^\nu}{\nu!},$$

and then derive approximated value for $F_{\lambda_n^*}(\lambda)$. Further, substituting $F_{\lambda_n^*}(\lambda - \phi)$ along with approximated PDF expression of the direct link $f_{\lambda_0}(\phi)$ into (9), we get approximated expression for $F_{\lambda_{S_i}}^{\infty}(\lambda)$ as

$$\begin{aligned}F_{\lambda_{S_i}}^{\infty}(\lambda) \simeq \sum_{n=0}^{N}\binom{N}{n}(-1)^n \sum_{k_1=0}^{n}\binom{n}{k_1}(-1)^{k_1}\sum_{k_2=0}^{n}\binom{n}{k_2} \\ \times(-1)^{k_2}\frac{\mu_1^{m_0}}{\Gamma(m_0)}\frac{1}{[\Gamma(m_{in}+1)]^{k_1}}\frac{1}{[\Gamma(m_{jn}+1)]^{k_2}} \\ \times\Big(\frac{m_{in}\tau_2}{\hat{\bar{\lambda}}_{in}}\Big)^{k_1 m_{in}}\Big(\frac{m_{jn}\tau_1}{\hat{\bar{\lambda}}_{jn}}\Big)^{k_2 m_{jn}} \\ \times B(m_0, k_1 m_{in} + k_2 m_{jn} + 1)\,\lambda^{m_0 + k_1 m_{in} + k_2 m_{jn}},\end{aligned} \tag{27}$$

where $B(\cdot, \cdot)$ represent Beta function. Substituting (27) into (14) and solving required integration, we get approximated MGF expression as

$$\begin{aligned}\mathscr{M}_{\lambda_{S_i}}^{\infty}(s) \simeq \sum_{n=0}^{N}\binom{N}{n}(-1)^n \sum_{k_1=0}^{n}\binom{n}{k_1}(-1)^{k_1}\sum_{k_2=0}^{n}\binom{n}{k_2} \\ \times(-1)^{k_2}\frac{\mu_1^{m_0}}{\Gamma(m_0)}\frac{1}{[\Gamma(m_{in}+1)]^{k_1}}\frac{1}{[\Gamma(m_{jn}+1)]^{k_2}} \\ \times\Big(\frac{m_{in}\tau_2}{\hat{\bar{\lambda}}_{in}}\Big)^{k_1 m_{in}}\Big(\frac{m_{jn}\tau_1}{\hat{\bar{\lambda}}_{jn}}\Big)^{k_2 m_{jn}} \\ \times B(m_0, k_1 m_{in} + k_2 m_{jn} + 1) \\ \times\Gamma(m_0 + k_1 m_{in} + k_2 m_{jn} + 1)\,\mathrm{s}^{m_0 + k_1 m_{in} + k_2 m_{jn}}.\end{aligned} \tag{28}$$

Further, we substitute (28) into (21) and derive the closed-form expression for $\mathscr{I}(\sqrt{\alpha}, \frac{\pi}{2})$, $\mathscr{I}(\sqrt{\frac{2\alpha}{3}}, \frac{\pi}{4})$, $\mathscr{I}(\sqrt{\alpha}, \frac{\pi}{2} - \arctan(\frac{1}{\sqrt{3}}))$, and $\mathscr{I}(\sqrt{\frac{\alpha}{3}}, \arctan(\frac{1}{\sqrt{3}}))$ by using (30)–(33) respectively, given in Appendix 1. Furthermore, by substituting these expressions into (20), asymptotic ASER expression for HQAM scheme can be obtained in Appendix 2 as shown in (40). From (40), we observe that the diversity order of the considered system depends on parameters such as N, m_0, m_{in}, m_{jn}, μ_1, τ_2, and τ_3. Parameters μ_1, τ_2, and τ_3 are directly related to CEE. Thus, for perfect CSI, the value of CEE is 0, and hence diversity order for the considered system is $m_0 + N \min(m_{in}, m_{jn})$. Further, when we consider imperfect CSI, $\sigma_{E_l}^2 = \sigma_{H_l}^2/(1 + \rho\bar{\lambda}_a\sigma_{H_l}^2) \to 0$ as $\bar{\lambda}_a \to \infty$. Hence, we can say that the CEE has no impact on the diversity order of the considered system.

4 Numerical and simulation results

In this section, we provide a comparison between ASER curves evaluated numerically by Mathematica, and Monte Carlo simulation for HQAM, RQAM, and XQAM schemes to validate our derived analytical expressions for the considered TWR 3P-ANC system. For analysis, we assume that the distance between source (S_i or S_j) and R_n, and also between two sources is d_l, $l \in \{in, jn, 0\}$. Thus, the average power of the Nakagami-m distributed link can be written as $\sigma_l^2 = 1/d_l^{a_0}$ where a linear network geometry $d_{in} + d_{jn} = 1$ is considered with $d_{in}, d_{jn} \in (0, 1)$ and path loss exponent $a_0 = 4$.

Fig. 2*a* and Fig. 2*b* show the comparison of theoretical, simulated, and asymptotic curves of ASER performance against transmit SNR for 8-HQAM scheme with imperfect CSI and perfect CSI cases, respectively, while considering the fading parameter $m_l = 1, 2$ and number of relays $N = 1, 2$. From the figures, we observe that simulated and theoretical curves match well with each other for $m_l = 1$, $N = 1$ which validates the correctness of the ASER expression of general order HQAM scheme. Further, alignment of asymptotic curves with the simulated and theoretical curves for ASER at high SNRs again validate the accuracy of the theoretical results. Furthermore, from the behaviour of simulated and theoretical curves, it can be observed that the gap between both the curves increases with the increase in m_l and N for a given SNR value. However, an improvement occurs for very high SNRs (> 25 dB). This observation indicates that the closed-form theoretical expressions can be a good approximation for small values of m_l and N. Although, ASER performance improves with the increase in m_l and N because of the improved diversity gain of the system which can be seen from slope of the curves. Moreover, from the figures, it can also be observed that ASER performance below 10 dB for each considered cases is not noteworthy even in better fading environment and also in the availability of more number of relays. However, in the moderate to high SNR regime, ASER performance improves significantly with variation in m_l from 1 to 2, and N from 1 to 2. For example, in the case of imperfect CSI, to maintain an ASER of 10^{-4}, the SNR gain of 7.6 dB (approx.) is observed when fading parameter (m_l) varies from 1 to 2 for $N = 1$, however, 6.5 dB (approx.) gain is observed when N increases from 1 to 2 for $m_l = 1$. Similarly, in case of perfect CSI, to maintain an ASER of 10^{-4}, 7.75 dB (approx.) SNR gain is observed when m_l varies from 1 to 2 and N is fixed at 1, and 6.75 dB (approx.) SNR gain is observed when N varies from 1 to 2 and m_l is fixed at 1.

Fig. 3*a* and Fig. 3*b* show comparative analysis of both theoretical and simulated curves of ASER performance against transmit SNR for 4×2-RQAM scheme with imperfect CSI and perfect CSI cases, respectively, while considering fading parameter $m_l = 1, 2$ and number of relay $N = 1, 2$. From the figures, it is observed that the impact of fading parameter and the number of relays on ASER performance for imperfect and perfect CSI follow similar trends as in Fig. 2*a* and Fig. 2*b*, respectively.

In Fig. 4*a* and Fig. 4*b*, comparison of theoretical and simulated curves of ASER performance against transmit SNR are illustrated for 32-XQAM scheme with imperfect and perfect CSI cases,

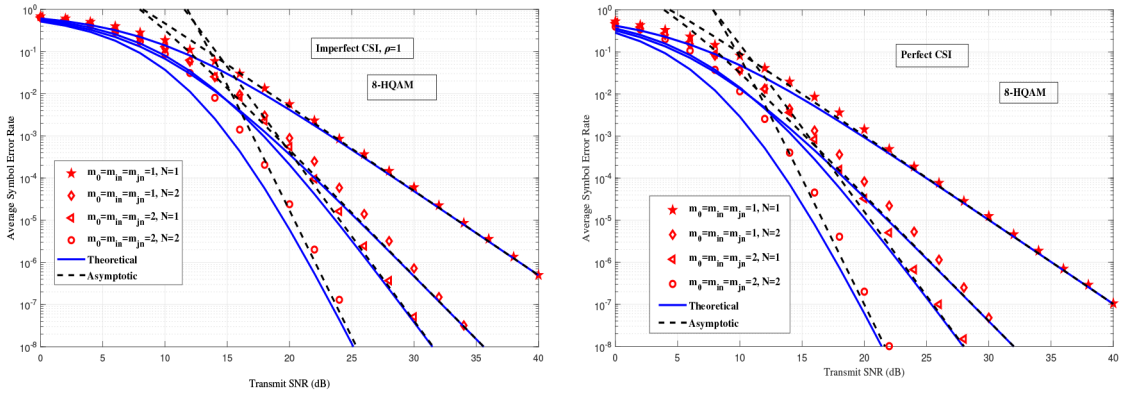

Fig. 2 *ASER performance of HQAM scheme versus transmit SNR for*
(a) Imperfect CSI, ***(b)*** Perfect CSI, under i.n.i.d. Nakagami-*m* faded scenario in two-way multi-relay network

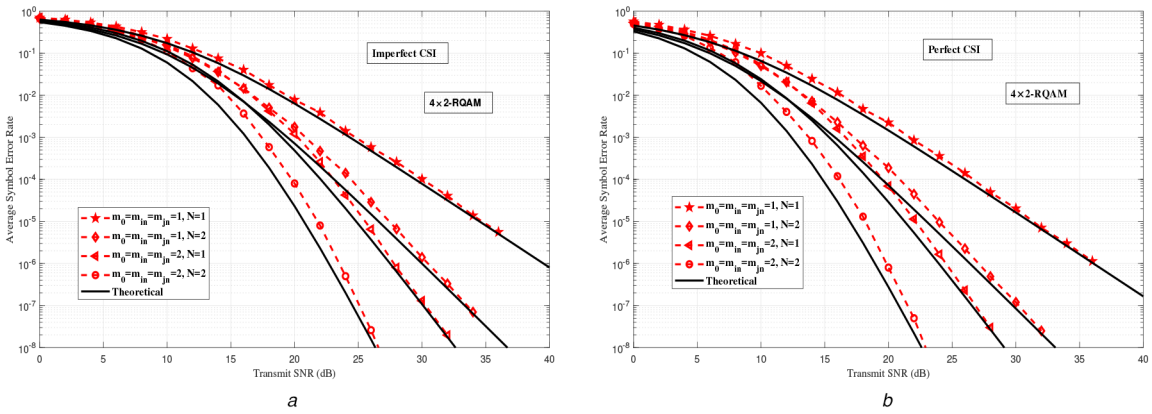

Fig. 3 *ASER performance of RQAM scheme versus transmit SNR for*
(a) Imperfect CSI, ***(b)*** Perfect CSI, under i.n.i.d. Nakagami-*m* faded scenario in two-way multi-relay network

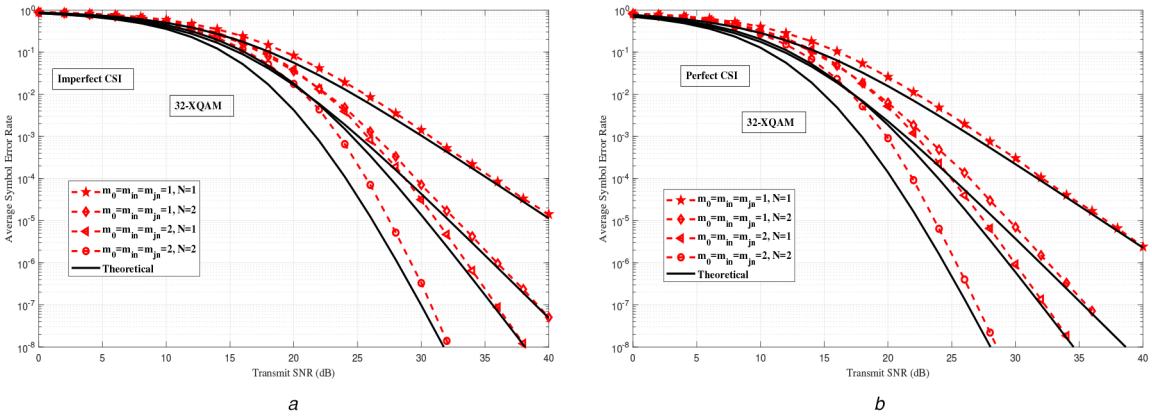

Fig. 4 *ASER performance of XQAM scheme versus transmit SNR for*
(a) Imperfect CSI, ***(b)*** Perfect CSI, under i.n.i.d. Nakagami-*m* faded scenario in two-way multi-relay network

respectively, while considering fading parameter $m_l = 1, 2$ and number of relay $N = 1, 2$. Again the curves of ASER performance for imperfect and perfect CSI follow similar trends as in Fig. 2*a* and Fig. 2*b*, respectively.

Fig. 5*a* and Fig. 5*b* illustrate comparative analysis of theoretical ASER performance for 8-HQAM scheme against normalised relay distance d_{in} with imperfect CSI and perfect CSI, respectively, when considering equal power distribution at source and relay nodes. From the figures, we can easily observe that the minimum ASER occurs at $d_{in} = 0.5$ when $m_l = 1, N = 1$ and $m_l = 2, N = 2$ (i.e. balanced channel conditions) for both imperfect and perfect CSI cases. However, for unequal values of m_{in} and m_{jn}, minimum ASER occurs at $d_{in} = 0.3$ or $d_{in} = 0.7$ irrespective of m_0 and N. This implies that the relay should be located near the source S_i or S_j for higher values of m_{jn} or m_{in}, respectively.

In Fig. 6, impact of number of relays on ASER performance over different SNR values for 4×2-RQAM constellation has been illustrated with imperfect CSI ($\rho = 1$), while considering fading parameter $m_l = 1$. From the figure, it is observed that the ASER performance improves with the increase in N (from 1 to 6) at each particular SNR value because of the improved diversity gain of the system.

Fig. 7 shows a comparative analysis of ASER results for 4×2-RQAM constellation for no relay and various cooperative relay cases. The ASER performance of 4×2-RQAM constellation for no relay case is analysed by substituting $N = 0$ in the derived generalised ASER expression of RQAM scheme as shown in (38). From the figure, we observe that to maintain an ASER of 10^{-2}, the SNR gain of 12.34 dB (approx.) is observed when N varies from 0 (without relay) to 1, however, 15.90 dB (approx.) and 17.55 dB

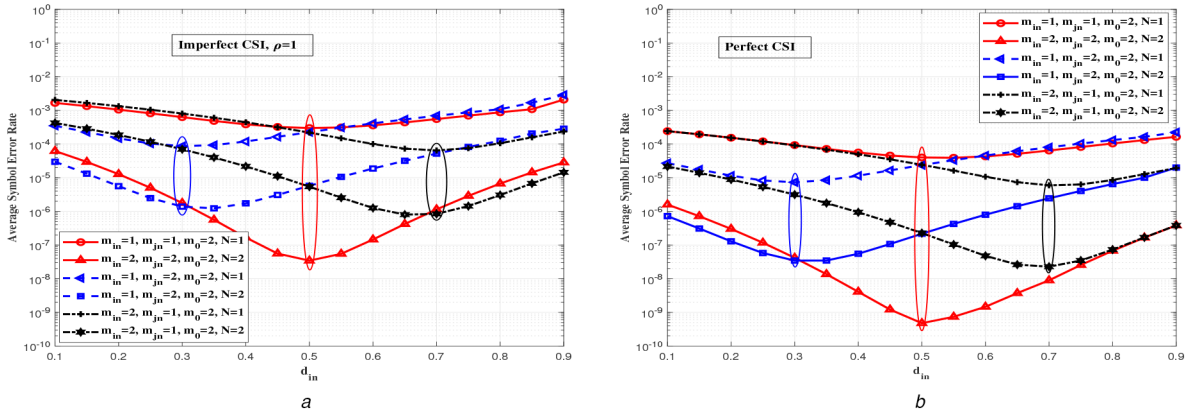

Fig. 5 *Comparative analysis of ASER for 8-HQAM versus normalised relay distance d_{in} for*
(a) Imperfect CSI, ***(b)*** Perfect CSI under i.n.i.d. Nakagami-*m* faded scenario in two-way multi-relay network

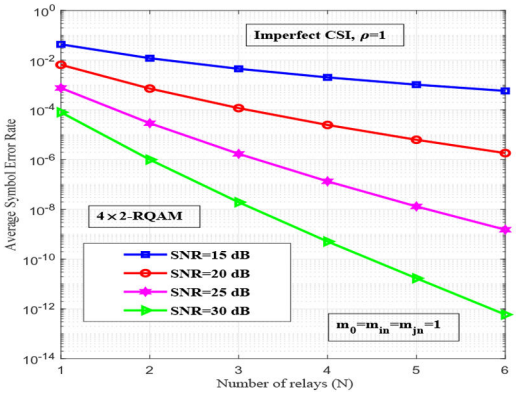

Fig. 6 *Comparative analysis of ASER performance for 4 × 2-RQAM constellation with a variation of number of relays (N)*

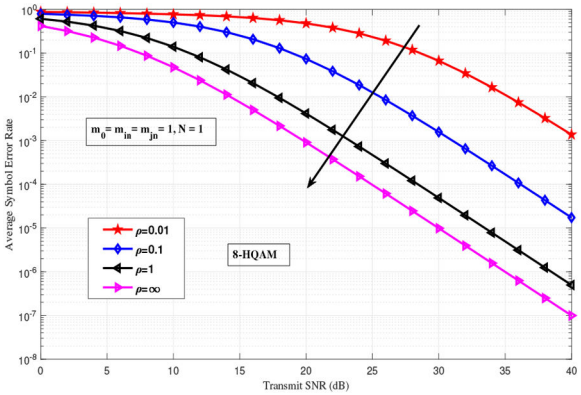

Fig. 8 *Comparative analysis of ASER performance for 8-HQAM constellation with a variation of ρ*

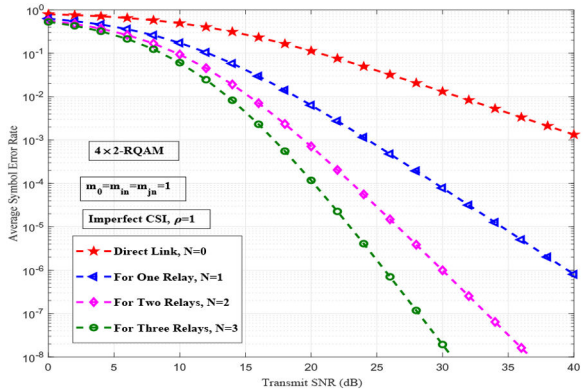

Fig. 7 *Comparative analysis of ASER performance for 4 × 2-RQAM constellation for no relay and various cooperative relay cases*

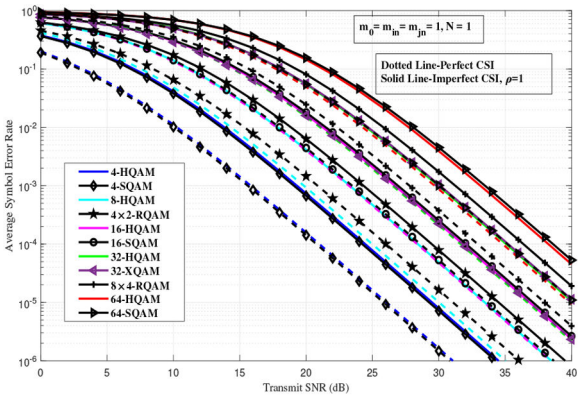

Fig. 9 *Comparative analysis of ASER performance for different QAM constellations versus transmit SNR*

gains are observed when N varies from 0 to 2 and 0 to 3, respectively. This is due to the fact that the diversity order is m_0 for no relay case which improves to $m_0 + N \min(m_{in}, m_{jn})$ for the considered cooperative relay case. From this observation we can say that the direct transmission from the two sources can be successfully decoded however by using relay links, the signal's strength and further ASER performance have been improved.

In Fig. 8, comparison of theoretical curves of ASER performance against transmit SNR for 8-HQAM scheme considering imperfect CSI ($\rho = 0.01, 0.1, 1$) and perfect CSI ($\rho = \infty$). It is observed that ASER performance improves with the increase in ρ. For the perfect CSI ($\rho \to \infty$), system achieves maximum ASER performance because of the maximum diversity order $m_0 + N \min(m_{in}, m_{jn})$. However, for the imperfect CSI, ASER performance improves with the increase in ρ but diversity order remains the same as found in Section 3.4. For instance, to maintain an ASER of 10^{-2}, the SNR gains of 9.50 dB (approx.), 7.75 dB (approx.), and 3.80 dB are observed when value of ρ increases from 0.01 to 0.1, 0.1 to 1, and 1 to ∞, respectively.

Fig. 9 illustrates the comparative analysis of theoretical ASER results for different QAM constellations considering imperfect and perfect CSI cases. From the figure, it is observed that the ASER performance of HQAM constellation for all the considered cases outperforms the SQAM, RQAM, and XQAM except for 4-QAM constellation. It is observed that 4-HQAM constellation provides slightly poorer performance than 4-SQAM because of the higher value of parameter $\mathscr{K}$. For higher constellation, HQAM performs better because of the higher value of parameter α and relatively low peak and average powers than SQAM, RQAM and, XQAM for both the perfect and imperfect CSI cases. For example, in the case of imperfect CSI, to maintain an ASER of 10^{-4}, 8-HQAM provides SNR gain of 1 dB (approx.) over 4 × 2-RQAM, 16-HQAM provides SNR gain of 0.30 dB (approx.) over 16-SQAM, 32-HQAM provides SNR gain of 1.20 dB (approx.) and 0.15 dB

(approx.) over 8×4-RQAM and 32-XQAM, respectively, and 64-HQAM provides SNR gain of 0.43 dB (approx.) over 64-SQAM. Similarly, in the case of perfect CSI, to maintain an ASER of 10^{-4}, 8-HQAM provides SNR gain of 1 dB (approx.) over 4×2-RQAM, 16-HQAM provides SNR gain of 0.33 dB (approx.) over 16-SQAM, 32-HQAM provides SNR gain of 1.25 dB (approx.) and 0.20 dB (approx.) over 8×4-RQAM and 32-XQAM, respectively, and 64-HQAM provides SNR gain of 0.45 dB (approx.) over 64-SQAM. However, for the 4-QAM constellation, SQAM provides SNR gain of 0.30 dB (approx.) and 0.25 dB (approx.) over HQAM in both imperfect and perfect CSI cases, respectively.

5 Conclusion

In this paper, closed-form expressions of ASER were derived for general order HQAM, RQAM, and XQAM schemes in a two-way multi-relay system using 3P-ANC considering both perfect and imperfect CSI under Nakagami-*m* fading channels. Further, asymptotic ASER expression was also obtained in high SNR regime to find the diversity order of the system. Furthermore, the impact of fading parameter, number of relays, CEE, and relay location on ASER performance, and usefulness of system diversity were also highlighted.

6 Acknowledgments

The authors thank the National Institute of Technology (NIT) Jamshedpur, MeitY's Visvesvaraya PhD scheme, and the Indian Institute of Technology (IIT) Indore, for all the support.

7 References

[1] Rankov, B., Wittneben, A.: 'Spectral efficient protocols for half-duplex relay channels', *IEEE J. Sel. Areas Commun.*, 2007, **25**, (2), pp. 379–389
[2] Yi, Z., Ju, M., Kim, I.-M.: 'Outage probability and optimum power allocation for analog network coding', *IEEE Trans. Wirel. Commun.*, 2011, **10**, (2), pp. 407–412
[3] Park, J.C., Song, I., Kim, Y.H.: 'Outage-optimal allocation of relay power for analog network coding with three transmission phases', *IEEE Commun. Lett.*, 2012, **16**, (6), pp. 838–841
[4] Bletsas, A., Khisti, A., Reed, D.P.*, et al.*: 'A simple cooperative diversity method based on network path selection', *IEEE J. Sel. Areas Commun.*, 2005, **24**, (3), pp. 659–672
[5] Song, L.: 'Relay selection for two-way relaying with amplify-and-forward protocols', *IEEE Trans. Veh. Technol.*, 2011, **60**, (4), pp. 1954–1959
[6] Ju, M., Kim, I.-M.: 'Relay selection with ANC and TDBC protocols in bidirectional relay networks', *IEEE Trans. Commun.*, 2010, **58**, (12), pp. 3500–3511
[7] Yadav, S., Upadhyay, P.K.: 'Performance of three-phase analog network coding with relay selection in Nakagami-*m* fading', *IEEE Commun. Lett.*, 2013, **17**, (8), pp. 1620–1623
[8] Wang, C., Liu, T.C.-K., Dong, X.: 'Impact of channel estimation error on the performance of amplify-and-forward two-way relaying', *IEEE Trans. Veh. Technol.*, 2012, **61**, (3), pp. 1197–1207
[9] Li, J., Ge, J., Zhang, C.*, et al.*: 'Impact of channel estimation error on bidirectional MABC-AF relaying with asymmetric traffic requirements', *IEEE Trans. Veh. Technol.*, 2013, **62**, (4), pp. 1755–1769
[10] Wang, L., Cai, Y., Yang, W.: 'On the finite-SNR DMT of two-way AF relaying with imperfect CSI', *IEEE Wirel. Commun. Lett.*, 2012, **1**, (3), pp. 161–164
[11] Singya, P.K., Kumar, N., Bhatia, V.: 'Performance analysis of opportunistic two-way 3P-ANC multi-relay system with imperfect CSI and NLPA'. IEEE Global Commun. Conf. (GLOBECOM), Abu Dhabi, United Arab Emirates, February 2019, pp. 206–212
[12] Yang, L., Qaraqe, K., Serpedin, E.*, et al.*: 'Performance analysis of amplify-and-forward two-way relaying with co-channel interference and channel estimation error', *IEEE Trans. Commun.*, 2013, **61**, (6), pp. 2221–2231
[13] Yadav, S., Upadhyay, P.K.: 'Finite-SNR diversity-multiplexing tradeoff for three-phase ANC with channel estimation errors', *IEEE Commun. Lett.*, 2014, **18**, (5), pp. 817–820
[14] Choi, D., Lee, J.: 'Outage probability of two-way full-duplex relaying with imperfect channel state information', *IEEE Commun. Lett.*, 2014, **18**, (6), pp. 933–936
[15] Li, C., Wang, H., Yao, Y.*, et al.*: 'Outage performance of the full-duplex two-way DF relay system under imperfect CSI', *IEEE Access*, 2017, **5**, pp. 5425–5435
[16] Mishra, A.K., Gowda, S.C.M., Singh, P.: 'Impact of hardware impairments on TWRN and OWRN AF relaying systems with imperfect channel estimates'. Proc. IEEE Wireless Communications and Networking Conf. (WCNC), San Francisco, USA, March 2017, pp. 1–6
[17] Yadav, S., Upadhyay, P.K.: 'Overall outage analysis of three-phase analog network coding with channel estimation errors'. Proc. IEEE 79th Vehicular Technology Conf., Seoul, South Korea, May 2014, pp. 1–5
[18] Mandpura, A., Prakriya, S., Mallik, R.K.: 'Outage probability of fixed-gain amplify-and-forward two-way relays with multiple co-channel interferers', *IET Commun.*, 2019, **13**, (6), pp. 649–656
[19] Abdelaziz, M., Gulliver, T.A.: 'Triangular constellations for adaptive modulation', *IEEE Trans. Commun.*, 2018, **66**, (2), pp. 756–766
[20] Dixit, D., Sahu, P.R.: 'Performance analysis of rectangular QAM with SC receiver over Nakagami-*m* fading channels', *IEEE Commun. Lett.*, 2014, **18**, (7), pp. 1262–1265
[21] Kumar, N., Singya, P.K., Bhatia, V.: 'ASER analysis of hexagonal and rectangular QAM schemes in multiple-relay networks', *IEEE Trans. Veh. Technol.*, 2018, **67**, (2), pp. 1815–1819
[22] Singya, P.K., Kumar, N., Bhatia, V.: 'Impact of imperfect CSI on ASER of hexagonal and rectangular QAM for AF relaying network', *IEEE Commun. Lett.*, 2018, **22**, (2), pp. 428–431
[23] Rugini, L.: 'Symbol error probability of hexagonal QAM', *IEEE Commun. Lett.*, 2016, **20**, (8), pp. 1523–1526
[24] Park, S.J.: 'Performance analysis of triangular quadrature amplitude modulation in AWGN channel', *IEEE Commun. Lett.*, 2012, **16**, (6), pp. 765–768
[25] Park, S.J., Byeon, M.-K.: 'Irregularly distributed triangular quadrature amplitude modulation'. IEEE 19th Int. Symp. on Personal Indoor and Mobile Radio Communication, Cannes, France, December 2008, pp. 1–5
[26] Park, S.J., Byeon, M.-K., Jeon, J.: 'Odd-bit triangular quadrature amplitude modulations'. IEEE 20th Int. Symp. on Personal, Indoor and Mobile Radio Commun., Tokyo, Japan, April 2010, pp. 2419–2423
[27] Yulong, Z., Wei, P.Z.: 'Relay-selection improves the security-reliability trade-off in cognitive radio systems', *IEEE Trans. Commun.*, 2015, **63**, (1), pp. 215–228
[28] Jia, Z., Yulong, Z., Wei, P.Z.*, et al.*: 'Security-reliability tradeoff analysis of multirelay-aided decode-and-forward cooperation systems', *IEEE Trans. Veh. Technol.*, 2016, **65**, (7), pp. 5825–5831
[29] Kumar, N., Singya, P.K., Bhatia, V.: 'Performance analysis of orthogonal frequency division multiplexing-based cooperative amplify-and-forward networks with non-linear power amplifier over independently but not necessarily identically distributed Nakagami-*m* fading channels', *IET Commun.*, 2017, **11**, (7), pp. 1008–1020
[30] Gradshteyn, I., Ryzhik, I.: '*Table of integrals, series and products*' (Academic, New York, NY, USA, 2000, 6th edn.)
[31] An, K., Lin, M., Ouyang, J.*, et al.*: 'Symbol error analysis of hybrid satellite-terrestrial cooperative networks with co-channel interference', *IEEE Commun. Lett.*, 2014, **18**, (11), pp. 1947–1950
[32] Simon, M.K., Alouini, M.-S.: '*Digital communication over fading channels*' (Wiley, Hoboken, NJ, USA, 2005, 2nd edn.)
[33] Dixit, D., Sahu, P.R.: 'Performance of QAM signaling over TWDP fading channels', *IEEE Trans. Wirel. Commun.*, 2013, **12**, (4), pp. 1794–1799

8 Appendix

8.1 Appendix 1

In this appendix, we derive the expression for $\mathcal{I}(\mathscr{C}, \phi)$ presented in (21).

1. *Derivation of* $\mathcal{I}(\chi, \frac{\pi}{2})$: From (21), we can write

$$\mathcal{I}\left(\chi, \frac{\pi}{2}\right) = \frac{1}{\pi}\int_0^{\pi/2} \mathscr{M}_{\lambda_{S_i}}\left(\frac{\chi^2}{2\sin^2\theta}\right) \mathrm{d}\theta \tag{29}$$

   Substituting (15) into (21) followed by changing the variable $z = \cos^2\theta$ and utilising the integral identity, we get (see (30)) .

2. *Derivation of* $\mathcal{I}(\chi, \frac{\pi}{4})$: Substituting (15) into (21) and adopting the change of variable $z = 1 - \tan^2\theta$ with utilising the integral

$$\begin{aligned}\mathcal{I}\left(\chi, \frac{\pi}{2}\right) = {} & \frac{1}{2\pi}\mathscr{M}_{\lambda_1}\left(\frac{\chi^2}{2}\right)\frac{\Gamma(\frac{1}{2})\Gamma(m_0+\frac{1}{2})}{\Gamma(m_0+1)}\,{}_2F_1\left(\frac{1}{2}, m_0, m_0+1; \frac{1}{1+\frac{\chi^2}{2\mu_1}}\right) + \frac{\Xi_1\Phi_1}{2\pi}\mathscr{M}_{\lambda_2}\left(\frac{\chi^2}{2}\right)\frac{\Gamma(\frac{1}{2})\Gamma(\ell_1-\frac{1}{2})}{\Gamma(\ell_1)} \\ & \times\, {}_2F_1\left(\frac{1}{2}, \ell_1, \ell_1; \frac{1}{1+\frac{\chi^2}{2n\mu_2}}\right) - \frac{\Xi_2\Phi_2}{2\pi}\mathscr{M}_{\lambda_3}\left(\frac{\chi^2}{2}\right)\frac{\Gamma(\frac{1}{2})\Gamma(\ell_2-\frac{1}{2})}{\Gamma(\ell_2)}\,{}_2F_1\left(\frac{1}{2}, \ell_2, \ell_2; \frac{1}{1+\frac{\chi^2}{2\mu_1}}\right).\end{aligned} \tag{30}$$

identity, we can obtain the closed-form expression for $\mathcal{I}(\chi, \frac{\pi}{4})$ as (see (31)) .

3. *Derivation of* $\mathcal{I}(\chi, \text{arccot}(y/x))$: Putting (15) into (21) then substituting $z = 1 - (y^2/x^2)\tan^2\theta$ and after simplifying the integration, the closed-form expression for $\mathcal{I}(\chi, \text{arccot}(y/x))$ can be expressed as (see (32)) .
4. *Derivation of* $\mathcal{I}(\chi, \arctan(\frac{y}{x}))$: Putting (15) into (21) further performing the change of variable $z = 1 - (x^2/y^2)\tan^2\theta$ and after simplification, the closed-form expression for $\mathcal{I}(\chi, \arctan(y/x))$ can be obtained as (see (33)) .
5. *Derivation of* $\mathcal{I}(\chi, \arctan(1/(2t+1)))$: Substituting (15) into (21) and adopting the change of variable $z = 1 - (2t+1)^2\tan^2\theta$ with further simplification, we can obtain the closed-form expression for $\mathcal{I}(\chi, \arctan(1/(2t+1)))$ as (see (34)) .
6. *Derivation of* $\mathcal{I}(\chi, \arctan(t(t+1)))$: Putting (15) into (21) then using the substituting $z = 1 - ((t+1)/t)^2\tan^2\theta$ and after simplification, the closed-form expression for $\mathcal{I}(\chi, \arctan(t/(t+1)))$ can be expressed as (see (35)) .
7. *Derivation of* $\mathcal{I}(\chi, \arctan(t/(t-1)))$: Substituting (15) into (21) and adopting the change of variable $z = 1 - (\frac{t-1}{t})^2\tan^2\theta$ with further simplification, we can obtain the closed-form expression for $\mathcal{I}(\chi, \arctan(\frac{t}{t-1}))$ as (see (36)) .

8.2 Appendix 2

In this section, we discuss the derivation of ASER expression for *M*-ary HQAM, *M*-ary RQAM, *M*-ary XQAM schemes, and asymptotic ASER analysis for *M*-ary HQAM scheme.

1. *M-ary HQAM:* By substituting expressions of $\mathcal{I}(\sqrt{\alpha}, \frac{\pi}{2})$, $\mathcal{I}(\sqrt{\frac{2\alpha}{3}}, \frac{\pi}{4})$, $\mathcal{I}(\sqrt{\alpha}, \frac{\pi}{2} - \arctan(\frac{1}{\sqrt{3}}))$, and $\mathcal{I}(\sqrt{\frac{\alpha}{3}}, \arctan(\frac{1}{\sqrt{3}}))$ (derived in Appendix 1) into (20) and simplifying the resulting expression, we can derive the closed-form expression of ASER for HQAM scheme as shown in (see (37)) .
2. *M-ary RQAM:* By substituting expressions of $\mathcal{I}(a, \frac{\pi}{2})$, $\mathcal{I}(b, \frac{\pi}{2})$, $\mathcal{I}(a, \frac{\pi}{2} - \arctan(\frac{b}{a}))$, and $\mathcal{I}(b, \arctan(\frac{b}{a}))$ (derived in Appendix 1) into (24), the ASER expression for *M*-ary RQAM scheme can be obtained as (see (38)) .
3. *M-ary XQAM:* By substituting expressions of $\mathcal{I}(\mathcal{A}_0, \frac{\pi}{2})$, $\mathcal{I}(\mathcal{A}_1, \frac{\pi}{2})$, $\mathcal{I}(\mathcal{A}_0, \frac{\pi}{4})$, $\mathcal{I}(\mathcal{A}_0, \kappa_t)$, $\mathcal{I}(\mathcal{A}_t, \omega_t^+)$, and $\mathcal{I}(\mathcal{A}_t, \omega_t^-)$ (derived in Appendix 1) into (26), the ASER expression for *M*-ary XQAM scheme can be obtained as (see (39)) .
4. *Asymptotic ASER:* By substituting expressions of $\mathcal{I}(\sqrt{\alpha}, \frac{\pi}{2})$, $\mathcal{I}(\sqrt{\frac{2\alpha}{3}}, \frac{\pi}{4})$, $\mathcal{I}(\sqrt{\alpha}, \frac{\pi}{2} - \arctan(\frac{1}{\sqrt{3}}))$, and $\mathcal{I}(\sqrt{\frac{\alpha}{3}}, \arctan(\frac{1}{\sqrt{3}}))$ (derived in Appendix 1) into (20), we can derive asymptotic ASER expression for HQAM scheme as shown in (see (40)) .

$$\mathcal{I}\left(\chi,\arctan\left(\frac{1}{2t+1}\right)\right)=\frac{2t+1}{(2t+1)^2+1}\Big[\frac{1}{2\pi}\mathcal{M}_{\lambda_1}\Big(\frac{\chi^2}{2}\Big[1+(2t+1)^2\Big]\Big)\frac{\Gamma(1)\Gamma(m_0+\frac{1}{2})}{\Gamma(m_0+\frac{3}{2})}\,F_1\Big(1,1,m_0;m_0+\frac{3}{2};\frac{1}{1+(2t+1)^2};$$
$$\frac{1+\frac{\chi^2}{2\mu_1}}{1+(1+(2t+1)^2)\frac{\chi^2}{2\mu_1}}\Big)+\frac{\Xi_1\Phi_1}{2\pi}\mathcal{M}_{\lambda_2}\Big(\frac{\chi^2}{2}\Big[1+(2t+1)^2\Big]\Big)\frac{\Gamma(1)\Gamma(\ell_1-\frac{1}{2})}{\Gamma(\ell_1+\frac{1}{2})}\,{}_2F_1\Big(1,\ell_1,\ell_1+\frac{1}{2};\frac{1+\frac{\chi^2}{2n\mu_2}}{1+(1+(2t+1)^2)\frac{\chi^2}{2n\mu_2}}\Big) \quad (34)$$
$$-\frac{\Xi_2\Phi_2}{2\pi}\mathcal{M}_{\lambda_3}\Big(\frac{\chi^2}{2}\Big[1+(2t+1)^2\Big]\Big)\frac{\Gamma(1)\Gamma(\ell_2-\frac{1}{2})}{\Gamma(\ell_2+\frac{1}{2})}\,{}_2F_1\Big(1,\ell_2,\ell_2+\frac{1}{2};\frac{1+\frac{\chi^2}{2\mu_1}}{1+(1+(2t+1)^2)\frac{\chi^2}{2\mu_1}}\Big)\Big].$$

$$\mathcal{I}\left(\chi,\arctan\left(\frac{t}{t+1}\right)\right)=\frac{(\frac{t+1}{t})}{1+(\frac{t+1}{t})^2}\Big[\frac{1}{2\pi}\mathcal{M}_{\lambda_1}\Big(\frac{\chi^2}{2}\Big[1+\Big(\frac{t+1}{t}\Big)^2\Big]\Big)\frac{\Gamma(1)\Gamma(m_0+\frac{1}{2})}{\Gamma(m_0+\frac{3}{2})}\,F_1\Big(1,1,m_0;m_0+\frac{3}{2};\frac{1}{1+(\frac{t+1}{t})^2};$$
$$\frac{1+\frac{\chi^2}{2\mu_1}}{1+(1+(\frac{t+1}{t})^2)\frac{\chi^2}{2\mu_1}}\Big)+\frac{\Xi_1\Phi_1}{2\pi}\mathcal{M}_{\lambda_2}\Big(\frac{\chi^2}{2}\Big[1+\Big(\frac{t+1}{t}\Big)^2\Big]\Big)\frac{\Gamma(1)\Gamma(\ell_1-\frac{1}{2})}{\Gamma(\ell_1+\frac{1}{2})}\,{}_2F_1\Big(1,\ell_1,\ell_1+\frac{1}{2};\frac{1+\frac{\chi^2}{2n\mu_2}}{1+(1+(\frac{t+1}{t})^2)\frac{\chi^2}{2n\mu_2}}\Big) \quad (35)$$
$$-\frac{\Xi_2\Phi_2}{2\pi}\mathcal{M}_{\lambda_3}\Big(\frac{\chi^2}{2}\Big[1+\Big(\frac{t+1}{t}\Big)^2\Big]\Big)\frac{\Gamma(1)\Gamma(\ell_2-\frac{1}{2})}{\Gamma(\ell_2+\frac{1}{2})}\,{}_2F_1\Big(1,\ell_2,\ell_2+\frac{1}{2};\frac{1+\frac{\chi^2}{2\mu_1}}{1+(1+(\frac{t+1}{t})^2)\frac{\chi^2}{2\mu_1}}\Big)\Big].$$

$$\mathcal{I}\left(\chi,\arctan\left(\frac{t}{t-1}\right)\right)=\frac{(\frac{t-1}{t})}{1+(\frac{t-1}{t})^2}\Big[\frac{1}{2\pi}\mathcal{M}_{\lambda_1}\Big(\frac{\chi^2}{2}\Big[1+\Big(\frac{t-1}{t}\Big)^2\Big]\Big)\frac{\Gamma(1)\Gamma(m_0+\frac{1}{2})}{\Gamma(m_0+\frac{3}{2})}\,F_1\Big(1,1,m_0;m_0+\frac{3}{2};\frac{1}{1+(\frac{t-1}{t})^2};$$
$$\frac{1+\frac{\chi^2}{2\mu_1}}{1+(1+(\frac{t-1}{t})^2)\frac{\chi^2}{2\mu_1}}\Big)+\frac{\Xi_1\Phi_1}{2\pi}\mathcal{M}_{\lambda_2}\Big(\frac{\chi^2}{2}\Big[1+\Big(\frac{t-1}{t}\Big)^2\Big]\Big)\frac{\Gamma(1)\Gamma(\ell_1-\frac{1}{2})}{\Gamma(\ell_1+\frac{1}{2})}\,{}_2F_1\Big(1,\ell_1,\ell_1+\frac{1}{2};\frac{1+\frac{\chi^2}{2n\mu_2}}{1+(1+(\frac{t-1}{t})^2)\frac{\chi^2}{2n\mu_2}}\Big) \quad (36)$$
$$-\frac{\Xi_2\Phi_2}{2\pi}\mathcal{M}_{\lambda_3}\Big(\frac{\chi^2}{2}\Big[1+\Big(\frac{t-1}{t}\Big)^2\Big]\Big)\frac{\Gamma(1)\Gamma(\ell_2-\frac{1}{2})}{\Gamma(\ell_2+\frac{1}{2})}\,{}_2F_1\Big(1,\ell_2,\ell_2+\frac{1}{2};\frac{1+\frac{\chi^2}{2\mu_1}}{1+(1+(\frac{t-1}{t})^2)\frac{\chi^2}{2\mu_1}}\Big)\Big].$$

$$\mathcal{I}\Big(\chi,\frac{\pi}{4}\Big)=\frac{1}{4\pi}\mathcal{M}_{\lambda_1}(\chi^2)\,\frac{\Gamma(1)\Gamma(m_0+\frac{1}{2})}{\Gamma(m_0+\frac{3}{2})}\,F_1\Big(1,1,m_0;m_0+\frac{3}{2};\frac{1}{2};\frac{1+\frac{\chi^2}{2\mu_1}}{1+\frac{\chi^2}{\mu_1}}\Big)+\frac{\Xi_1\Phi_1}{4\pi}\mathcal{M}_{\lambda_2}(\chi^2)\,\frac{\Gamma(1)\Gamma(\ell_1-\frac{1}{2})}{\Gamma(\ell_1+\frac{1}{2})}$$
$$\times\ {}_2F_1\Big(1,\ell_1,\ell_1+\frac{1}{2};\frac{1+\frac{\chi^2}{2n\mu_2}}{1+\frac{\chi^2}{n\mu_2}}\Big)-\frac{\Xi_2\Phi_2}{4\pi}\mathcal{M}_{\lambda_3}(\chi^2)\,\frac{\Gamma(1)\Gamma(\ell_2-\frac{1}{2})}{\Gamma(\ell_2+\frac{1}{2})}\,{}_2F_1\Big(1,\ell_2,\ell_2+\frac{1}{2};\frac{1+\frac{\chi^2}{2\mu_1}}{1+\frac{\chi^2}{\mu_1}}\Big). \quad (31)$$

$$\mathcal{I}\left(\chi,\operatorname{arccot}\left(\frac{y}{x}\right)\right)=\frac{xy}{(x^2+y^2)}\Big[\frac{1}{2\pi}\mathcal{M}_{\lambda_1}\Big(\frac{\chi^2}{2}\Big[\frac{x^2+y^2}{x^2}\Big]\Big)\frac{\Gamma(1)\Gamma(m_0+\frac{1}{2})}{\Gamma(m_0+\frac{3}{2})}\,F_1\Big(1,1,m_0;m_0+\frac{3}{2};\frac{x^2}{x^2+y^2};\frac{1+\frac{\chi^2}{2\mu_1}}{1+(\frac{x^2+y^2}{x^2})\frac{\chi^2}{2\mu_1}}\Big)$$
$$+\frac{\Xi_1\Phi_1}{2\pi}\mathcal{M}_{\lambda_2}\Big(\frac{\chi^2}{2}\Big[\frac{x^2+y^2}{x^2}\Big]\Big)\,\frac{\Gamma(1)\Gamma(\ell_1-\frac{1}{2})}{\Gamma(\ell_1+\frac{1}{2})}\,{}_2F_1\Big(1,\ell_1,\ell_1+\frac{1}{2};\frac{1+\frac{\chi^2}{2n\mu_2}}{1+(\frac{x^2+y^2}{x^2})\frac{\chi^2}{2n\mu_2}}\Big)+\frac{\Xi_2\Phi_2}{2\pi}\mathcal{M}_{\lambda_3}\Big(\frac{\chi^2}{2}\Big[\frac{x^2+y^2}{x^2}\Big]\Big) \quad (32)$$
$$\times\ \frac{\Gamma(1)\Gamma(\ell_2-\frac{1}{2})}{\Gamma(\ell_2+\frac{1}{2})}\,{}_2F_1\Big(1,\ell_2,\ell_2+\frac{1}{2};\frac{1+\frac{\chi^2}{2\mu_1}}{1+(\frac{x^2+y^2}{x^2})\frac{\chi^2}{2\mu_1}}\Big)\Big].$$

$$\mathcal{I}\left(\chi,\arctan\left(\frac{y}{x}\right)\right)=\frac{xy}{(x^2+y^2)}\Big[\frac{1}{2\pi}\mathcal{M}_{\lambda_1}\Big(\frac{\chi^2}{2}\Big[\frac{x^2+y^2}{y^2}\Big]\Big)\frac{\Gamma(1)\Gamma(m_0+\frac{1}{2})}{\Gamma(m_0+\frac{3}{2})}\,F_1\Big(1,1,m_0;m_0+\frac{3}{2};\frac{y^2}{x^2+y^2};\frac{1+\frac{\chi^2}{2\mu_1}}{1+(\frac{x^2+y^2}{y^2})\frac{\chi^2}{2\mu_1}}\Big)$$
$$+\frac{\Xi_1\Phi_1}{2\pi}\mathcal{M}_{\lambda_2}\Big(\frac{\chi^2}{2}\Big[\frac{x^2+y^2}{y^2}\Big]\Big)\,\frac{\Gamma(1)\Gamma(\ell_1-\frac{1}{2})}{\Gamma(\ell_1+\frac{1}{2})}\,{}_2F_1\Big(1,\ell_1,\ell_1+\frac{1}{2};\frac{1+\frac{\chi^2}{2n\mu_2}}{1+(\frac{x^2+y^2}{y^2})\frac{\chi^2}{2n\mu_2}}\Big)+\frac{\Xi_2\Phi_2}{2\pi}\mathcal{M}_{\lambda_3}\Big(\frac{\chi^2}{2}\Big[\frac{x^2+y^2}{y^2}\Big]\Big) \quad (33)$$
$$\times\ \frac{\Gamma(1)\Gamma(\ell_2-\frac{1}{2})}{\Gamma(\ell_2+\frac{1}{2})}\,{}_2F_1\Big(1,\ell_2,\ell_2+\frac{1}{2};\frac{1+\frac{\chi^2}{2\mu_1}}{1+(\frac{x^2+y^2}{y^2})\frac{\chi^2}{2\mu_1}}\Big)\Big].$$

$$
\begin{aligned}
P_{\mathrm{s}}^{\mathrm{HQAM}}(e) = {} & \frac{\mathscr{K}}{2\pi}\Big[\mathscr{M}_{\lambda_1}\Big(\frac{\alpha}{2}\Big)\,\frac{\Gamma(\frac{1}{2})}{\Gamma(m_0+\frac{1}{2})}\Gamma(m_0+1)\,{}_2F_1\Big(\frac{1}{2},m_0,m_0+1;\frac{1}{1+\frac{\alpha}{2\mu_1}}\Big)+\Xi_1\Phi_1\mathscr{M}_{\lambda_2}\Big(\frac{\alpha}{2}\Big)\,\frac{\Gamma(\frac{1}{2})\Gamma(\ell_1-\frac{1}{2})}{\Gamma(\ell_1)} \\
& \times {}_2F_1\Big(\frac{1}{2},\ell_1,\ell_1;\frac{1}{1+\frac{\alpha}{2n\mu_2}}\Big)-\Xi_2\Phi_2\mathscr{M}_{\lambda_3}\Big(\frac{\alpha}{2}\Big)\,\frac{\Gamma(\frac{1}{2})\Gamma(\ell_2-\frac{1}{2})}{\Gamma(\ell_2)}\,{}_2F_1\Big(\frac{1}{2},\ell_2,\ell_2;\frac{1}{1+\frac{\alpha}{2\mu_1}}\Big)\Big] \\
& +\frac{\mathscr{K}_c}{6\pi}\Big[\mathscr{M}_{\lambda_1}\Big(\frac{2\alpha}{3}\Big)\,\frac{\Gamma(1)\Gamma(m_0+\frac{1}{2})}{\Gamma(m_0+\frac{3}{2})}\,F_1\Big(1,1,m_0;m_0+\frac{3}{2};\frac{1}{2};\frac{1+\frac{\alpha}{3\mu_1}}{1+\frac{2\alpha}{3\mu_1}}\Big)+\Xi_1\Phi_1\mathscr{M}_{\lambda_2}\Big(\frac{2\alpha}{3}\Big)\,\frac{\Gamma(1)\Gamma(\ell_1-\frac{1}{2})}{\Gamma(\ell_1+\frac{1}{2})} \\
& \times {}_2F_1\Big(1,\ell_1,\ell_1+\frac{1}{2};\frac{1+\frac{\alpha}{3n\mu_2}}{1+\frac{2\alpha}{3n\mu_2}}\Big)-\Xi_2\Phi_2\mathscr{M}_{\lambda_3}\Big(\frac{2\alpha}{3}\Big)\,\frac{\Gamma(1)\Gamma(\ell_2-\frac{1}{2})}{\Gamma(\ell_2+\frac{1}{2})}\,{}_2F_1\Big(1,\ell_2,\ell_2+\frac{1}{2};\frac{1+\frac{\alpha}{3\mu_1}}{1+\frac{2\alpha}{3\mu_1}}\Big)\Big] \\
& -\frac{\sqrt{3}\mathscr{K}_c}{8\pi}\Big\{\mathscr{M}_{\lambda_1}\Big(\frac{2\alpha}{3}\Big)\frac{\Gamma(1)\Gamma(m_0+\frac{1}{2})}{\Gamma(m_0+\frac{3}{2})}\Big[\,F_1\Big(1,1,m_0;m_0+\frac{3}{2};\frac{1}{4};\frac{1+\frac{\alpha}{6\mu_1}}{1+\frac{2\alpha}{3\mu_1}}\Big)+\,F_1\Big(1,1,m_0;m_0+\frac{3}{2};\frac{3}{4};\frac{1+\frac{\alpha}{2\mu_1}}{1+\frac{2\alpha}{3\mu_1}}\Big)\Big] \\
& +\Xi_1\Phi_1\mathscr{M}_{\lambda_2}\Big(\frac{2\alpha}{3}\Big)\,\frac{\Gamma(1)\Gamma(\ell_1-\frac{1}{2})}{\Gamma(\ell_1+\frac{1}{2})}\Big[{}_2F_1\Big(1,\ell_1,\ell_1+\frac{1}{2};\frac{1+\frac{\alpha}{2n\mu_2}}{1+\frac{2\alpha}{3n\mu_2}}\Big)+{}_2F_1\Big(1,\ell_1,\ell_1+\frac{1}{2};\frac{1+\frac{\alpha}{6n\mu_2}}{1+\frac{2\alpha}{3n\mu_2}}\Big)\Big] \\
& -\Xi_2\Phi_2\mathscr{M}_{\lambda_3}\Big(\frac{2\alpha}{3}\Big)\,\frac{\Gamma(1)\Gamma(\ell_2-\frac{1}{2})}{\Gamma(\ell_2+\frac{1}{2})}\Big[{}_2F_1\Big(1,\ell_2,\ell_2+\frac{1}{2};\frac{1+\frac{\alpha}{2\mu_1}}{1+\frac{2\alpha}{3\mu_1}}\Big)+{}_2F_1\Big(1,\ell_2,\ell_2+\frac{1}{2};\frac{1+\frac{\alpha}{6\mu_1}}{1+\frac{2\alpha}{3\mu_2}}\Big)\Big]\Big\}.
\end{aligned}
\tag{37}
$$

$$
\begin{aligned}
P_{\mathrm{s}}^{\mathrm{RQAM}}(e) = {} & \frac{p}{\pi}\Big[\mathscr{M}_{\lambda_1}\Big(\frac{a^2}{2}\Big)\,\frac{\Gamma(\frac{1}{2})\Gamma(m_0+\frac{1}{2})}{\Gamma(m_0+1)}\,{}_2F_1\Big(\frac{1}{2},m_0,m_0+1;\frac{1}{1+\frac{a^2}{2\mu_1}}\Big)+\Xi_1\Phi_1\mathscr{M}_{\lambda_2}\Big(\frac{a^2}{2}\Big)\,\frac{\Gamma(\frac{1}{2})\Gamma(\ell_1-\frac{1}{2})}{\Gamma(\ell_1)} \\
& \times {}_2F_1\Big(\frac{1}{2},\ell_1,\ell_1;\frac{1}{1+\frac{a^2}{2n\mu_2}}\Big)-\Xi_2\Phi_2\mathscr{M}_{\lambda_3}\Big(\frac{a^2}{2}\Big)\,\frac{\Gamma(\frac{1}{2})\Gamma(\ell_2-\frac{1}{2})}{\Gamma(\ell_2)}\,{}_2F_1\Big(\frac{1}{2},\ell_2,\ell_2;\frac{1}{1+\frac{a^2}{2\mu_1}}\Big)\Big]+\frac{q}{\pi}\Big[\mathscr{M}_{\lambda_1}\Big(\frac{b^2}{2}\Big) \\
& \times\frac{\Gamma(\frac{1}{2})\Gamma(m_0+\frac{1}{2})}{\Gamma(m_0+1)}\,{}_2F_1\Big(\frac{1}{2},m_0,m_0+1;\frac{1}{1+\frac{b^2}{2\mu_1}}\Big)+\Xi_1\Phi_1\mathscr{M}_{\lambda_2}\Big(\frac{b^2}{2}\Big)\,\frac{\Gamma(\frac{1}{2})\Gamma(\ell_1-\frac{1}{2})}{\Gamma(\ell_1)}\,{}_2F_1\Big(\frac{1}{2},\ell_1,\ell_1;\frac{1}{1+\frac{b^2}{2n\mu_2}}\Big) \\
& -\Xi_2\Phi_2\mathscr{M}_{\lambda_3}\Big(\frac{b^2}{2}\Big)\,\frac{\Gamma(\frac{1}{2})\Gamma(\ell_2-\frac{1}{2})}{\Gamma(\ell_2)}\,{}_2F_1\Big(\frac{1}{2},\ell_2,\ell_2;\frac{1}{1+\frac{b^2}{2\mu_1}}\Big)\Big]-\frac{p\,q}{\pi}\frac{a\,b}{a^2+b^2}\Big\{\mathscr{M}_{\lambda_1}\Big(\frac{a^2+b^2}{2}\Big)\,\frac{\Gamma(1)\Gamma(m_0+\frac{1}{2})}{\Gamma(m_0+\frac{3}{2})} \\
& \times\Big[\,F_1\Big(1,1,m_0;m_0+\frac{3}{2};\frac{a^2}{a^2+b^2};\frac{1+\frac{a^2}{2\mu_1}}{1+\frac{a^2+b^2}{2\mu_1}}\Big)+\,F_1\Big(1,1,m_0;m_0+\frac{3}{2};\frac{b^2}{a^2+b^2};\frac{1+\frac{b^2}{2\mu_1}}{1+\frac{a^2+b^2}{2\mu_1}}\Big)\Big] \\
& +\Xi_1\Phi_1\mathscr{M}_{\lambda_2}\Big(\frac{a^2+b^2}{2}\Big)\,\frac{\Gamma(1)\Gamma(\ell_1-\frac{1}{2})}{\Gamma(\ell_1+\frac{1}{2})}\Big[{}_2F_1\Big(1,\ell_1,\ell_1+\frac{1}{2};\frac{1+\frac{a^2}{2n\mu_2}}{1+\frac{a^2+b^2}{2n\mu_2}}\Big)+{}_2F_1\Big(1,\ell_1,\ell_1+\frac{1}{2};\frac{1+\frac{b^2}{2n\mu_2}}{1+\frac{a^2+b^2}{2n\mu_2}}\Big)\Big] \\
& -\Xi_2\Phi_2\mathscr{M}_{\lambda_3}\Big(\frac{a^2+b^2}{2}\Big)\,\frac{\Gamma(1)\Gamma(\ell_2-\frac{1}{2})}{\Gamma(\ell_2+\frac{1}{2})}\Big[{}_2F_1\Big(1,\ell_2,\ell_2+\frac{1}{2};\frac{1+\frac{a^2}{2\mu_1}}{1+\frac{a^2+b^2}{2\mu_1}}\Big)+{}_2F_1\Big(1,\ell_1,\ell_1+\frac{1}{2};\frac{1+\frac{b^2}{2\mu_1}}{1+\frac{a^2+b^2}{2\mu_1}}\Big)\Big]\Big\}.
\end{aligned}
\tag{38}
$$

$$
\begin{aligned}
P_{\mathrm{s}}^{\mathrm{XQAM}}(e) = {} & \frac{\mathscr{U}}{2\pi}\Big[\mathscr{M}_{\lambda_1}\Big(\frac{\mathscr{A}_0^2}{2}\Big)\,\frac{\Gamma(\frac{1}{2})\Gamma(m_0+\frac{1}{2})}{\Gamma(m_0+1)}\,{}_2F_1\Big(\frac{1}{2},m_0,m_0+1;\frac{1}{1+\frac{\mathscr{A}_0^2}{2\mu_1}}\Big)+\Xi_1\Phi_1\mathscr{M}_{\lambda_2}\Big(\frac{\mathscr{A}_0^2}{2}\Big)\,\frac{\Gamma(\frac{1}{2})\Gamma(\ell_1-\frac{1}{2})}{\Gamma(\ell_1)}\\
& \times {}_2F_1\Big(\frac{1}{2},\ell_1,\ell_1;\frac{1}{1+\frac{\mathscr{A}_0^2}{2n\mu_2}}\Big)-\Xi_2\Phi_2\mathscr{M}_{\lambda_3}\Big(\frac{\mathscr{A}_0^2}{2}\Big)\,\frac{\Gamma(\frac{1}{2})\Gamma(\ell_2-\frac{1}{2})}{\Gamma(\ell_2)}\,{}_2F_1\Big(\frac{1}{2},\ell_2,\ell_2;\frac{1}{1+\frac{\mathscr{A}_0^2}{2\mu_1}}\Big)\Big]\\
& +\frac{2}{\pi M}\Big[\mathscr{M}_{\lambda_1}\big(\mathscr{A}_0^2\big)\,\frac{\Gamma(\frac{1}{2})\Gamma(m_0+\frac{1}{2})}{\Gamma(m_0+1)}\,{}_2F_1\Big(\frac{1}{2},m_0,m_0+1;\frac{1}{1+\frac{\mathscr{A}_1^2}{2\mu_1}}\Big)\Big]-\frac{\mathscr{V}}{4\pi}\Big[\mathscr{M}_{\lambda_1}(\mathscr{A}_0^2)\,\frac{\Gamma(1)\Gamma(m_0+\frac{1}{2})}{\Gamma(m_0+\frac{3}{2})}\\
& \times\ F_1\Big(1,1,m_0;m_0+\frac{3}{2};\frac{1}{2};\frac{1+\frac{\mathscr{A}_0^2}{2\mu_1}}{1+\frac{\mathscr{A}_0^2}{\mu_1}}\Big)+\Xi_1\Phi_1\mathscr{M}_{\lambda_2}(\mathscr{A}_0^2)\,\frac{\Gamma(1)\Gamma(\ell_1-\frac{1}{2})}{\Gamma(\ell_1+\frac{1}{2})}\,{}_2F_1\Big(1,\ell_1,\ell_1+\frac{1}{2};\frac{1+\frac{\mathscr{A}_0^2}{2n\mu_2}}{1+\frac{\mathscr{A}_0^2}{n\mu_2}}\Big)\\
& -\Xi_2\Phi_2\mathscr{M}_{\lambda_3}(\mathscr{A}_0^2)\,\frac{\Gamma(1)\Gamma(\ell_2-\frac{1}{2})}{\Gamma(\ell_2+\frac{1}{2})}\,{}_2F_1\Big(1,\ell_2,\ell_2+\frac{1}{2};\frac{1+\frac{\mathscr{A}_0^2}{2\mu_1}}{1+\frac{\mathscr{A}_0^2}{\mu_1}}\Big)\Big]-\frac{4}{\pi M}\sum_{t=1}^{\nu-1}\frac{2\mathrm{t}+1}{(2\mathrm{t}+1)^2+1}\\
& \times\Big\{\mathscr{M}_{\lambda_1}\Big(\frac{\mathscr{A}_0^2}{2}\Big[1+(2\mathrm{t}+1)^2\Big]\Big)\frac{\Gamma(1)\Gamma(m_0+\frac{1}{2})}{\Gamma(m_0+\frac{3}{2})}\,F_1\Big(1,1,m_0;m_0+\frac{3}{2};\frac{1}{1+(2\mathrm{t}+1)^2};\frac{1+\frac{\mathscr{A}_0^2}{2\mu_1}}{1+(1+(2\mathrm{t}+1)^2)\frac{\mathscr{A}_0^2}{2\mu_1}}\Big)\\
& +\Xi_1\Phi_1\mathscr{M}_{\lambda_2}\Big(\frac{\mathscr{A}_0^2}{2}\Big[1+(2\mathrm{t}+1)^2\Big]\Big)\frac{\Gamma(1)\Gamma(\ell_1-\frac{1}{2})}{\Gamma(\ell_1+\frac{1}{2})}\,{}_2F_1\Big(1,\ell_1,\ell_1+\frac{1}{2};\frac{1+\frac{\mathscr{A}_0^2}{2n\mu_2}}{1+(1+(2\mathrm{t}+1)^2)\frac{\mathscr{A}_0^2}{2n\mu_2}}\Big)\\
& -\Xi_2\Phi_2\mathscr{M}_{\lambda_3}\Big(\frac{\mathscr{A}_0^2}{2}\Big[1+(2\mathrm{t}+1)^2\Big]\Big)\frac{\Gamma(1)\Gamma(\ell_2-\frac{1}{2})}{\Gamma(\ell_2+\frac{1}{2})}\,{}_2F_1\Big(1,\ell_2,\ell_2+\frac{1}{2};\frac{1+\frac{\mathscr{A}_0^2}{2\mu_1}}{1+(1+(2\mathrm{t}+1)^2)\frac{\mathscr{A}_0^2}{2\mu_1}}\Big)\Big\}-\frac{2}{\pi M}\sum_{t=1}^{\nu-1}\frac{(\frac{\mathrm{t}+1}{t})}{1+(\frac{\mathrm{t}+1}{t})^2}\\
& \times\Big\{\mathscr{M}_{\lambda_1}\Big(\frac{\mathscr{A}_t}{2}\Big[1+\Big(\frac{\mathrm{t}+1}{t}\Big)^2\Big]\Big)\frac{\Gamma(1)\Gamma(m_0+\frac{1}{2})}{\Gamma(m_0+\frac{3}{2})}\,F_1\Big(1,1,m_0;m_0+\frac{3}{2};\frac{1}{1+(\frac{\mathrm{t}+1}{t})^2};\frac{1+\frac{\mathscr{A}_t}{2\mu_1}}{1+(1+(\frac{\mathrm{t}+1}{t})^2)\frac{\mathscr{A}_t}{2\mu_1}}\Big)\\
& +\Xi_1\Phi_1\mathscr{M}_{\lambda_2}\Big(\frac{\mathscr{A}_t}{2}\Big[1+\Big(\frac{\mathrm{t}+1}{t}\Big)^2\Big]\Big)\frac{\Gamma(1)\Gamma(\ell_1-\frac{1}{2})}{\Gamma(\ell_1+\frac{1}{2})}\,{}_2F_1\Big(1,\ell_1,\ell_1+\frac{1}{2};\frac{1+\frac{\mathscr{A}_t^2}{2n\mu_2}}{1+(1+(\frac{\mathrm{t}+1}{t})^2)\frac{\mathscr{A}_t^2}{2n\mu_2}}\Big)\\
& -\Xi_2\Phi_2\mathscr{M}_{\lambda_3}\Big(\frac{\mathscr{A}_t}{2}\Big[1+\Big(\frac{\mathrm{t}+1}{t}\Big)^2\Big]\Big)\frac{\Gamma(1)\Gamma(\ell_2-\frac{1}{2})}{\Gamma(\ell_2+\frac{1}{2})}\,{}_2F_1\Big(1,\ell_2,\ell_2+\frac{1}{2};\frac{1+\frac{\mathscr{A}_t^2}{2\mu_1}}{1+(1+(\frac{\mathrm{t}+1}{t})^2)\frac{\mathscr{A}_t^2}{2\mu_1}}\Big)\Big\}+\frac{2}{\pi M}\sum_{t=2}^{\nu}\frac{(\frac{\mathrm{t}-1}{t})}{1+(\frac{\mathrm{t}-1}{t})^2}\\
& \times\Big\{\mathscr{M}_{\lambda_1}\Big(\frac{\mathscr{A}_t^2}{2}\Big[1+\Big(\frac{\mathrm{t}-1}{t}\Big)^2\Big]\Big)\frac{\Gamma(1)\Gamma(m_0+\frac{1}{2})}{\Gamma(m_0+\frac{3}{2})}\,F_1\Big(1,1,m_0;m_0+\frac{3}{2};\frac{1}{1+(\frac{\mathrm{t}-1}{t})^2};\frac{1+\frac{\mathscr{A}_t^2}{2\mu_1}}{1+(1+(\frac{\mathrm{t}-1}{t})^2)\frac{\mathscr{A}_t^2}{2\mu_1}}\Big)\\
& +\Xi_1\Phi_1\mathscr{M}_{\lambda_2}\Big(\frac{\mathscr{A}_t^2}{2}\Big[1+\Big(\frac{\mathrm{t}-1}{t}\Big)^2\Big]\Big)\frac{\Gamma(1)\Gamma(\ell_1-\frac{1}{2})}{\Gamma(\ell_1+\frac{1}{2})}\,{}_2F_1\Big(1,\ell_1,\ell_1+\frac{1}{2};\frac{1+\frac{\mathscr{A}_t^2}{2n\mu_2}}{1+(1+(\frac{\mathrm{t}-1}{t})^2)\frac{\mathscr{A}_t^2}{2n\mu_2}}\Big)\\
& -\Xi_2\Phi_2\mathscr{M}_{\lambda_3}\Big(\frac{\mathscr{A}_t^2}{2}\Big[1+\Big(\frac{\mathrm{t}-1}{t}\Big)^2\Big]\Big)\frac{\Gamma(1)\Gamma(\ell_2-\frac{1}{2})}{\Gamma(\ell_2+\frac{1}{2})}\,{}_2F_1\Big(1,\ell_2,\ell_2+\frac{1}{2};\frac{1+\frac{\mathscr{A}_t^2}{2\mu_1}}{1+(1+(\frac{\mathrm{t}-1}{t})^2)\frac{\mathscr{A}_t^2}{2\mu_1}}\Big)\Big\}.
\end{aligned}
\tag{39}
$$

$$
\begin{aligned}
P_{\mathrm{s}}^{\infty}(e) \approx & \sum_{n=0}^{N}\binom{N}{n}(-1)^{n}\sum_{k_1=0}^{n}\binom{n}{k_1}(-1)^{k_1}\sum_{k_2=0}^{n}\binom{n}{k_2}(-1)^{k_2}\frac{\mu_1^{m_0}}{\Gamma(m_0)}\frac{1}{[\Gamma(m_{in}+1)]^{k_1}}\frac{1}{[\Gamma(m_{jn}+1)]^{k_2}}\Big(\frac{m_{in}\tau_2}{\hat{\bar{\lambda}}_{in}}\Big)^{k_1 m_{in}} \\
& \times\Big(\frac{m_{jn}\tau_1}{\hat{\bar{\lambda}}_{jn}}\Big)^{k_2 m_{jn}}\mathrm{B}(m_0, k_1 m_{in}+k_2 m_{jn}+1)\,\Gamma(m_0+k_1 m_{in}+k_2 m_{jn}+1)\Big\{\frac{\mathcal{K}}{2\pi}\Big(\frac{\alpha}{2}\Big)^{-(m_0+k_1 m_{in}+k_2 m_{jn})} \\
& \times\mathrm{B}\Big(m_0+k_1 m_{in}+k_2 m_{jn}+\frac{1}{2},\frac{1}{2}\Big)+\Big(\frac{2\alpha}{3}\Big)^{-(m_0+k_1 m_{in}+k_2 m_{jn})}\frac{\Gamma(1)\Gamma(m_0+k_1 m_{in}+k_2 m_{jn}+\frac{1}{2})}{\Gamma(m_0+k_1 m_{in}+k_2 m_{jn}+\frac{3}{2})} \\
& \times\Big[\frac{\mathcal{K}_c}{6\pi}{}_2F_1\Big(1, m_0+k_1 m_{in}+k_2 m_{jn}+1, m_0+k_1 m_{in}+k_2 m_{jn}+\frac{3}{2};\frac{1}{2}\Big) \\
& -\frac{\sqrt{3}\mathcal{K}_c}{8\pi}\Big({}_2F_1\Big(1, m_0+k_1 m_{in}+k_2 m_{jn}+1, m_0+k_1 m_{in}+k_2 m_{jn}+\frac{3}{2};\frac{3}{4}\Big) \\
& +{}_2F_1\Big(1, m_0+k_1 m_{in}+k_2 m_{jn}+1, m_0+k_1 m_{in}+k_2 m_{jn}+\frac{3}{2};\frac{1}{4}\Big)\Big)\Big]\Big\}.
\end{aligned}
\tag{40}
$$